Effective Frenkel Hamiltonian for optical nonlinearities in semiconductors: Application to magnetoexcitons

V. Chernyak, S. Yokojima, T. Meier, and S. Mukamel
Department of Chemistry and Rochester Theory Center for Optical Science and Engineering, University of Rochester, Rochester, New York 14627
(Received 10 November 1997; revised manuscript received 7 April 1998)

Closed Green-function expressions for the third-order response of semiconductors are derived by mapping the two-band model onto the much simpler molecular (Frenkel) Hamiltonian. The signatures of two-exciton resonances are incorporated through the exciton scattering matrix, totally avoiding the explicit calculation of two-exciton states. Exact expressions for the nonlinear optical response of two-dimensional semiconductor nanostructures in a strong perpendicular magnetic field are derived by truncating at the $n=1$ Landau level, and using the symmetry of the system and a group-theoretical analysis. We find that the nonlinear optical response depends crucially on asymmetries between particle-particle and particle-hole Coulomb interactions. [S0163-1829(98)03732-1]

I. INTRODUCTION

The influence of geometric confinement on the optical properties of semiconductor nanostructures has been investigated extensively over the past decade.[1–5] It is well established that exciton confinement on length scales smaller than its Bohr radius leads to increased exciton binding energies and larger oscillator strengths, and consequently to a stronger resonant optical response. These effects have been studied in quasi-two-dimensional, one-dimensional, and zero-dimensional systems (quantum wells, wires, and dots, respectively).[1–4] In addition to geometric confinement, the dimensionality of semiconductor systems may also be reduced by applying external fields. A strong static electric field applied in the growth direction of semiconductor superlattices suppresses the coupling between the quantum wells of the superlattice, resulting in a Stark localization of charge carriers[6] and changing the exciton from anisotropic three dimensional to basically two dimensional.[7] The same reduction of the effective exciton dimensionality can be induced by applying an appropriately chosen alternating field (*dynamic localization*).[8] Strong confinement effects on the relative electron-hole motion have also been achieved by applying static and homogeneous magnetic fields, which restrict the free motion of electrons perpendicular to the field, and lead to the formation of Landau levels.[9–14]

In a strong magnetic field one can neglect processes which involve transitions of an electron or a hole between different Landau levels. In this approximation, when exciton states are formed, relative electron-hole motion is only possible in the direction of the field. This implies that, in three-dimensional structures, strong magnetic fields result in one-dimensional relative motion,[9–11] while relative motion in two-dimensional semiconductors in strong perpendicular magnetic fields becomes zero dimensional.[12–14] In semiconductor quantum wells in a strong magnetic field, we have a single exciton for a given value of the center of mass momentum once the Landau levels of the electron and the hole are fixed.

Linear and nonlinear optical properties of magnetoexcitons in both bulk semiconductors[9–11,15] and in quantum wells[12–14] have been extensively studied experimentally. On the theoretical side, investigations of the linear spectra of magnetoexcitons in quantum wells[16] have pointed out the importance of valence-band mixing effects. Semiconductor Bloch equations (SBE's) for magnetoexcitons in two[17] and three[18] dimensions have been developed. The SBE's, which further allow the analysis of nonlinear optical properties, have been used to investigate many-particle effects, which in two dimensions results in coupling between the individual Landau states, and in three dimensions also in a coupling of higher-energy Landau states to the continuum of lower Landau states. This gives rise to Fano resonances in the linear spectra that exhibit a unique and not yet fully understood four-wave-mixing (FWM) response.[9,10] Calculations of FWM signal at Fano resonances neglecting many-particle effects[19] indicate that those should be responsible for the experimental findings.

Similar to the field-free case, it is crucial to include the many-particle Coulomb interaction for a proper description of the linear and especially the nonlinear optical properties of magnetoexcitons. The SBE's are based on the time-dependent Hartree-Fock (TDHF) approximation, where two-exciton variables are not included as independent variables.[2,20–22] They have been successfully applied to explain nonlinear optical phenomena in semiconductors and semiconductor nanostructures.[2] Recently, the importance of including correlations beyond the TDHF has been demonstrated mainly by analyzing the dependence of the nonlinear response on the polarization of the exciting pulses. The experimental findings have been explained in terms of excitation-induced dephasing processes[23–26] which were related to excitonic screening. It has been shown that these terms are related to the two exciton continuum,[27–29] i.e., result from exciton-exciton scattering. The role of bound biexcitons in four-wave mixing on semiconductors has been further pointed out.[28,30–36] Recently, using a polarization configuration that eliminates the contribution of bound biexcitons, the signatures of unbound two-exciton states on four-

wave mixing signals from GaAs layers have been investigated both experimentally and theoretically.[11]

Similar problems appear in optical excitations of molecular crystals and nanostructures which are represented by the Frenkel exciton Hamiltonian. The role of two-exciton states in the third-order optical response of Frenkel-exciton systems has been well understood.[37] The analog of the SBE for Frenkel-exciton systems has been called the local-field approximation (LFA),[37] and can be derived by taking the expectation value of the Heisenberg equation of motion for excitons operators and factorizing the expectation values of higher-order products into products of expectation values of exciton operators, which yields a closed system of equations for one-exciton variables.[37] The LFA accounts for exciton-exciton scattering, and gives correct results far from the two-photon resonances on two-exciton states. These equations have been generalized by introducing closed equations of motion for one- and two-exciton variables,[38] which yields exact results for the third-order optical response in the absence of dephasing, and shows the limitations of the LFA. This formalism is based on the fact that correlation functions can be classified according to their order in the exciting field. This allows a systematic truncation of the many-body problem at a given order in the fields. The third-order response functions was later rederived using the concept of exciton-exciton scattering[39] which finally resulted in Green-function expressions for $\chi^{(3)}$.[40] $\chi^{(3)}$ is then represented as a product of four one-exciton Green functions and the exciton-exciton scattering matrix. Radiative damping has been also incorporated.[41] Coupled equations of motion for one-exciton, and exciton population variables which take into account dephasing induced by exciton-phonon coupling, were developed in Ref. 42. This theory provides an adequate description of degenerate four-wave mixing, where population relaxation is of extreme importance; however, treating exciton-exciton scattering on the LFA level does not reproduce two-exciton resonances explicitly. The approach of Ref. 43, which deals with coupled equations of motion for one-exciton, two-exciton, and exciton-population variables interpolates between the theories of Refs. 38 and 42; however, it does not describe the combined effects of exciton population relaxation and resonant exciton-exciton scattering.

The LFA has been generalized to include population relaxation and resonant exciton-exciton scattering. A theory which accounts for these combined effects developed in Ref. 44 is based on Green-function techniques and perturbative treatment of exciton-phonon interaction with partial infinite resummation of perturbative contributions. This theory has been applied to interpret pump-probe measurements in photosynthetic antenna complexes.[45] An alternative, more intuitive, derivation is based on a closed system of coupled equations for one-exciton, two-exciton, exciton-population, and combined one-plus-two-exciton coherence variables eliminating the phonons using projection operator techniques,[46] and applying certain factorization to relaxation kernels rather than to exciton variables.[44]

Recent developments in semiconductors follow precisely the same line of thought: the $\chi^{(3)}$ formalism developed to include correlations beyond the TDHF in semiconductor systems[27,47–51] manifests itself in a straightforward generalization of the theory of Refs. 2 and 38. This has been demonstrated[52] by mapping the two-band semiconductor Hamiltonian onto an effective exciton model. By establishing the connection between the two models, we can apply many of the results developed for Frenkel systems to semiconductors. The Frenkel Hamiltonian restricts the dynamics of the two-band model to a relevant subset of states. By doing so the problem is simplified considerably, making it easier to develop higher levels of theories which include correlation, scattering and phonon effects.

In this paper, starting with a two-band model, we use the formal similarity between semiconductor and molecular systems to derive closed equations of motion for one- and two-exciton variables which are exact for up to third-order nonlinear optical response. By solving these equations perturbatively in the external field we obtain compact Green-function expressions (GFE's) for the third-order susceptibility. Using a formalism originally developed for Frenkel-exciton systems, $\chi^{(3)}$ is expressed in terms of one-exciton Green functions and the exciton-exciton scattering matrix which accounts for two-photon resonances on two-exciton states. These expressions include the effects of both bound and unbound two-exciton states. We apply GFE's to calculate $\chi^{(3)}$ of two-dimensional magnetoexcitons in the limit of strong magnetic fields, where we can restrict the calculation to the lowest $(n=1)$ Landau exciton. Using the symmetry of the system, a group-theoretical analysis enables us to derive exact expressions for the optical response including both bound and unbound two-exciton states. Calculating the two-exciton states is a four-particle problem, which in two dimensions means that the wave functions depend on eight coordinates. Neglecting the small photon momentum, only two-exciton states with zero total momentum can be excited, which reduces the number of coordinates to six. In strong magnetic fields we can restrict the analysis to the $n=1$ Landau level, and eliminate the relative motion of the electron-hole pair. The two-exciton states with zero momentum are then constructed out of pairs of one-exciton states from the lowest Landau level with opposite center-of-mass momenta, and the calculation of these states involves only two coordinates. We do not have to consider trial-variational wave functions for the two-exciton states, and no further approximations are necessary beyond making use of the symmetries of the system and truncating at the $n=1$ Landau level, which in strong magnetic fields is energetically well separated from all other higher-lying levels. It was shown previously that the thermodynamical properties of spinless magnetoexcitons depend crucially on asymmetries between the particle-particle and particle-hole Coulomb interactions.[53] In particular, if these two interactions are identical, an ensemble of magnetoexcitons at low concentrations behaves like an ensemble of noninteracting bosons.[54] We will show that there is still a finite nonlinear optical response in this case. We extend these theories by considering excitons with different angular momenta, and investigate the spectra of two-exciton states for different ratios of the various Coulomb interactions. By solving the equations of motion derived here, we predict the signatures of two-exciton states in nonlinear optical experiments conducted on GaAs quantum wells in strong magnetic fields.

As in the absence of a magnetic field, polarization-dependent two- and three-pulse FWM experiments in which

the signal is analyzed for different polarization configurations of the exciting pulses are most likely to pinpoint the influence of two-exciton states on the nonlinear optical response. In such experiments two-exciton states with different symmetries may be investigated separately by varying the polarizations of the excitation pulses. Here we focus on the frequency-domain two-color pump-probe signal.

This paper is organized as follows. In Sec. II, the two-band Hamiltonian of semiconductors is mapped onto a Frenkel exciton system which is exact up to the third order of the optical response. The Hamiltonian is used to derive the equations of motion for one- and two-exciton variables in Sec. III. Using these equations of motion, the Green-function expressions for the third-order optical susceptibility are derived. In order to apply the Hamiltonian to a quantum well in a strong magnetic field, in Sec. IV we calculate relevant one- and two-exciton states. Here we choose the Coulomb potential in a form which accounts for the asymmetry in the particle-particle and particle-hole interactions. Closed expressions for the third-order susceptibility of magnetoexcitons are given in Sec. V. Numerical results are presented in Sec. VI. Energies of the two-exciton eigenstates show various distributions depending on different asymmetries of the Coulomb interaction. Using the expression for the third-order susceptibility of magnetoexcitons, two-color pump-probe signals are calculated. The signal strongly depends on asymmetries of the Coulomb interaction.

II. MAPPING THE TWO-BAND HAMILTONIAN ONTO A FRENKEL FORM

We start with the two-band model Hamiltonian of semiconductors[52]

$$\begin{aligned} H=&\sum_{m_1n_1} t^{(1)}_{m_1n_1} a^\dagger_{m_1} a_{n_1} + \sum_{m_2n_2} t^{(2)}_{m_2n_2} b^\dagger_{m_2} b_{n_2} \\ &+\tfrac{1}{2}\sum_{m_1n_1k_1l_1} V^{(1)}_{m_1n_1k_1l_1} a^\dagger_{m_1} a^\dagger_{n_1} a_{k_1} a_{l_1} \\ &+\tfrac{1}{2}\sum_{m_2n_2k_2l_2} V^{(2)}_{m_2n_2k_2l_2} b^\dagger_{m_2} b^\dagger_{n_2} b_{k_2} b_{l_2} \\ &+\tfrac{1}{2}\sum_{m_1n_2k_2l_1} W_{m_1n_2l_1k_2} a^\dagger_{m_1} b^\dagger_{n_2} b_{k_2} a_{l_1}. \end{aligned} \tag{2.1}$$

Here a_{n_1} ($a^\dagger_{n_1}$) and the b_{n_2} ($b^\dagger_{n_2}$) are the Fermi annihilation (creation) operators of electrons and holes respectively, with the commutation relations

$$\begin{aligned} a_{n_1}a^\dagger_{m_1} + a^\dagger_{m_1}a_{n_1} &= \delta_{m_1n_1}, \\ b_{n_2}b^\dagger_{m_2} + b^\dagger_{m_2}b_{n_2} &= \delta_{m_2n_2}. \end{aligned} \tag{2.2}$$

We adopt the following convention for indices: Latin indices with a subscript 1 (2), e.g., m_1 (m_2) stand for electron (holes), including spin variables. Electron-hole pairs are denoted by Latin indices without subscripts $m=(m_1m_2)$.

The Hamiltonian of the system $H_T(\tau)$ in the presence of the driving field $\mathcal{E}(\mathbf{r},\tau)$ has the form

$$H_T(\tau) = H - \int d\mathbf{r}\ \mu(\mathbf{r})\mathcal{E}(\mathbf{r},\tau), \tag{2.3}$$

with the dipole operator

$$\mu(\mathbf{r}) \equiv \sum_{m_1m_2} \mu_{m_1m_2}(\mathbf{r})(a^\dagger_{m_1}b^\dagger_{m_2} + b_{m_2}a_{m_1}). \tag{2.4}$$

Following Ref. 52, we introduce the electron-hole operators

$$B^\dagger_{m_1m_2} \equiv a^\dagger_{m_1}b^\dagger_{m_2}, \quad B_{m_1m_2} \equiv b_{m_2}a_{m_1}, \tag{2.5}$$

and expand the Hamiltonian [Eq. (2.1)] in powers of normally ordered B and $B^\dagger$ operators, retaining all terms up to the fourth order, which are needed for calculating the optical response up to the third order. This yields

$$H = \sum_{mn} h_{mn}B^\dagger_m B_n + \tfrac{1}{2}\sum_{mnkl} \Gamma_{mn,kl}B^\dagger_m B^\dagger_n B_k B_l. \tag{2.6}$$

Expressions for the matrices h_{mn} and $\Gamma_{mn,kl}$ in terms of the parameters of the original Hamiltonian Eq. (2.1) are given in Refs. 52. A similar expansion yields for the commutation relations[52]

$$[B_m, B^\dagger_n] = \delta_{mn} - 2\sum_{pq} P_{mp,nq}B^\dagger_p B_q, \tag{2.7}$$

with $P=\frac{1}{2}[P^{(1)}+P^{(2)}]$ and $P^{(1)}[P^{(2)}]$ being the electron (hole) permutation operators.

It is important to emphasize that the Hamiltonian and commutation relations written in terms of exciton operators [Eqs. (2.6) and (2.7)] generally contain an infinite power series of $B^\dagger$ and B operators. However, only a finite number of terms contribute to the optical response at a given order in the field. In Eqs. (2.6) and (2.7) we only retained the terms that contribute to the third-order response. In order to calculate higher-order response we need to include additional higher-order products in the expansion of both the Hamiltonian and the commutators.

Making use of Eqs. (2.6) and (2.7), the Heisenberg equation of motion for electron-hole operators $i dB_n/d\tau = [B_n, H]$ yields

$$\begin{aligned} i\frac{dB_n}{d\tau} =& \sum_m h_{nm}B_m - \mathcal{E}_n + \sum_{mpq} U_{nm,pq}B^\dagger_m B_p B_q \\ &+ \sum_{mpq} P_{nm,pq}B^\dagger_m(B_p\mathcal{E}_q + B_q\mathcal{E}_p), \end{aligned} \tag{2.8}$$

where

$$\mathcal{E}_n \equiv \int d\mathbf{r}\ \mu_n(\mathbf{r})\mathcal{E}(\mathbf{r}), \tag{2.9}$$

and μ_n is the polarization of the nth electron-hole pair. h is an operator acting in the one-exciton space whose eigenvalues give the one-exciton energies:[52]

$$h = t^{(1)}\otimes I + I\otimes t^{(2)} + W. \tag{2.10}$$

The first two terms on the right-hand side of Eq. (2.10) represent the kinetic energy of an electron and a hole, whereas the last term represents the electron-hole Coulomb interac-

tion. The operator U acting in the two-exciton space is represented by a tetradic matrix $U_{nm,pq}$, and describes exciton-exciton Coulomb interactions

$$U=V_{13}^{(1)}+V_{24}^{(2)}+W_{14}+W_{32}. \tag{2.11}$$

In Eq. (2.11) we used the following convention: the two-exciton space can be represented as $(V_1\otimes V_2)\otimes(V_3\otimes V_4)$, where $V_1=V_3=V$ is the electron space, whereas $V_2=V_4=V^*$ is the hole space, and $V_1\otimes V_2$ and $V_3\otimes V_4$ represent two identical replicas of the single-exciton space. For any operator Q acting in $V_i\otimes V_j$, we denote by Q_{ij} an operator in the two-exciton space which acts as Q in $V_i\otimes V_j$ and as a unit operator in the product of the remaining two single-particle spaces.

The first two terms on the right-hand side of Eq. (2.11) represent electron-electron and hole-hole interactions, whereas the third term represents the electron-hole interactions. Note that electron-hole Coulomb energy for an electron and a hole which belong to the same exciton is included in h but does not appear in U. The tetradic matrix $P_{nm,pq}$ in Eq. (2.8) also represents a two-exciton operator.

Equations (2.8) are not closed, and a proper truncation procedure needs to be developed in order to convert them into a practical computational method. In the simplest truncation scheme, known as the local-field approximation, we factorize all products of normal ordered operators into single operator expectation values. This yields a closed equation for the expectation values.

$$i\frac{d\langle B_n\rangle}{d\tau}=\sum_m h_{nm}\langle B_m\rangle-\mathcal{E}_n+\sum_{mpq}U_{nm,pq}\langle B_m\rangle^*\langle B_p\rangle\langle B_q\rangle$$

$$+\sum_{mpq}P_{nm,pq}\langle B_m\rangle^*(\langle B_p\rangle\mathcal{E}_q+\langle B_q\rangle\mathcal{E}_p). \tag{2.12}$$

Equation (2.12) constitutes the LFA for the exciton Hamiltonian of Eq. (2.6) and is equivalent to the SBE for the two-band model written in terms of exciton operators introduced by Eq. (2.5). Note that since Eq. (2.12) was derived using Eqs. (2.6) and (2.7), it is equivalent to the SBE up to the third-order response, and should be modified when higher-order response functions are calculated.

The same equation [Eq. (2.12)] was derived in Ref. 55 for the model of a Frenkel-exciton aggregate made of three-level molecules. In that case Latin indices represent the molecules, and $B_n(B_n^\dagger)$ are Frenkel exciton annihilation (creation) operators in the molecular representation. We assume that each molecule has three electronic levels, where $\Omega_n^{(1)}$ and $\Omega_n^{(2)}$ are the transition frequencies between consecutive levels (Fig. 1). We further denote the ratio between consecutive transition dipoles of the mth molecules by κ_m. Expressions for h, U, and P were given in Ref. 55. We then have

$$U_{mn,kl}=\delta_{mn}\tfrac{1}{2}[\delta_{mk}\delta_{nl}g_m+(\kappa_m^2-2)\times(h_{mk}\delta_{nl}+\delta_{mk}h_{nl})]P_{mn,kl}, \tag{2.13}$$

with

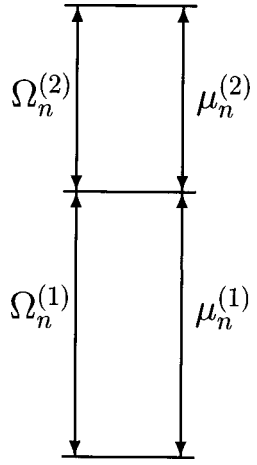

FIG. 1. The optical response of the two-band model of semiconductors calculated using semiconductor Bloch equations (SBE's) can be mapped onto an effective lattice of three-level systems described by the Frenkel Hamiltonian. The parameters of this simpler model are given in this figure. Two sources of nonlinearity (anharmonicity) are identified [$\kappa\equiv\mu_n^{(2)}/\mu_n^{(1)}$ and g (Eq. (2.13)].

$$g_n=2\Omega_n^{(2)}\kappa_n^{-2}-\Omega_n^{(1)},$$

$$P_{mnkl}=\delta_{mn}\delta_{m\kappa}\delta_{nk}\left(1-\frac{\kappa_m^2}{2}\right).$$

Neglecting the momentum of the optical field, Eq. (2.12) is reduced to the equation of motion for the zero-momentum exciton operators $\psi\equiv\Sigma_m B_m$, which assumes the form of the Ginzburg-Landau equation

$$i\frac{d\psi}{d\tau}=\Omega\psi-\mu\mathcal{E}+V|\psi|^2\psi+\mu b|\psi|^2\mathcal{E}. \tag{2.14}$$

Equation (2.14) applies to both the Frenkel exciton model and the semiconductor two-band model. Within these approximations the third-order response is characterized by the ratio V/b, which determines the relative importance of the two optical nonlinearities. For the two-band model, the parameters V and b are determined by the shape of the one-exciton wave function. Taking $\phi(\mathbf{k})$ to be the real wave function of the $1s$ exciton in $\mathbf{k}$ space (here $\mathbf{k}$ is the momentum associated with the relative motion of electrons and holes), and denoting the Coulomb-interaction by $V(\mathbf{k}-\mathbf{k}')$, the two nonlinear terms are given by[56,57]

$$b=2\sum_{\mathbf{k}}\phi(\mathbf{k})^3, \tag{2.15}$$

$$V=2\sum_{\mathbf{k},\mathbf{k}'}V(\mathbf{k}-\mathbf{k}')[\phi(\mathbf{k})^3\phi(\mathbf{k}')-\phi(\mathbf{k})^2\phi(\mathbf{k}')^2]. \tag{2.16}$$

(Similar equations in real space were given in Ref. 58.) b represents phase-space filling, and V denotes the Coulomb interaction. b is always finite, with a value which is determined by the exciton wave function. In contrast, the expression for V [Eq. (2.16)] involves a difference between two terms, and the sign of V can be different for different wave functions.

For the effective Frenkel exciton model we obtain, from Eq. (2.13),

$$b=2-\kappa^2, \qquad V=(\kappa^2-2)h+\frac{\kappa^2 g}{2}. \tag{2.17}$$

Now b represents non-Bose statistics, whereas V depends on statistics as well as anharmonicity.

III. COUPLED ONE- AND TWO-EXCITON DYNAMICS; THIRD-ORDER SUSCEPTIBILITIES BEYOND THE LFA

In this section we make use of Eqs. (2.6) and (2.7) to derive equations of motion for one- and two-exciton variables, whose solution results in closed expressions for the third-order susceptibility which goes beyond the local-field approximation. In the absence of pure dephasing, the pure state factorization can be applied, and Eq. (2.8) leads to the following closed equations of motion for one- and two-exciton variables:[52]

$$i\frac{d\langle B_n\rangle}{d\tau}=\sum_m h_{nm}\langle B_m\rangle-\mathcal{E}_n+\sum_{mpq}U_{nm,pq}\langle B_m^\dagger\rangle\langle B_pB_q\rangle + \sum_{mpq}P_{nm,pq}\langle B_m^\dagger\rangle(\langle B_p\rangle\mathcal{E}_q+\langle B_q\rangle\mathcal{E}_p), \tag{3.1}$$

$$i\frac{d\langle B_nB_{n'}\rangle}{d\tau}-\sum_{mm'}(h_{nm}\delta_{n'm'}+\delta_{nm}h_{n'm'})\langle B_mB_{m'}\rangle - \sum_{mm'}U_{nn',mm'}\langle B_mB_{m'}\rangle = -(\delta_{nm}\delta_{n'm'}-P_{nn',mm'})(\mathcal{E}_m\langle B_{m'}\rangle+\langle B_m\rangle\mathcal{E}_{m'}). \tag{3.2}$$

These equations are exact for the response up to third order, and are equivalent to the equations derived in Ref. 47–49.

Equations (3.1) and (3.2) can be solved perturbatively in the external field. Switching to the frequency domain yields Green function expressions for optical susceptibilities which may be conveniently represented by introducing operator notation. For the linear susceptibility we have

$$\chi^{(1)}(-\omega\mathbf{r}_s;\omega\mathbf{r})=\langle\mu(\mathbf{r}_s)|R^{(1)}(-\omega;\omega)|\mu(\mathbf{r})\rangle, \tag{3.3}$$

where $\mu(\mathbf{r})$ is treated as a vector in the one-exciton space with components $\mu_n(\mathbf{r})$, whereas $R^{(1)}$ is an operator in the same space:

$$R^{(1)}(-\omega;\omega)=G(\omega)+G^\dagger(-\omega). \tag{3.4}$$

$G(\omega)$ is the one-exciton Green function

$$G(\omega)=[(\omega+i\eta)I-h]^{-1}, \tag{3.5}$$

where η is phenomenological damping.

The GFE for the third-order susceptibility has the form

$$\chi^{(3)}(-\omega_s\mathbf{r}_s;\omega_1\mathbf{r}_1,\omega_2\mathbf{r}_2,-\omega_3\mathbf{r}_3) = \tfrac{1}{6}\sum_{perm}\langle\mu(\mathbf{r}_s)\otimes\mu(\mathbf{r}_3)|R(-\omega_s;\omega_1,\omega_2,-\omega_3)| \times\mu(\mathbf{r}_1)\otimes\mu(\mathbf{r}_2)\rangle+\text{c.c.}, \tag{3.6}$$

where Σ_{perm} denotes a sum over the six permutations of three pairs $\omega_1\mathbf{r}_1,\omega_2\mathbf{r}_2$, and $-\omega_3\mathbf{r}_3$. The operator R acting in the two-exciton space is given by

$$R(-\omega_s;\omega_1,\omega_2,-\omega_3)=G(\omega_s)\otimes G^\dagger(\omega_3)\overline{\Gamma}(\omega_1+\omega_2)G(\omega_1)\otimes G(\omega_2), \tag{3.7}$$

where the two-exciton scattering matrix, treated as an operator in two-exciton space, has the form

$$\overline{\Gamma}(\omega)=-2P[\overline{F}(\omega)]^{-1}+2U\{[\overline{F}(\omega)]^{-1}-U\}^{-1} \times(I-P)[\overline{F}(\omega)]^{-1}, \tag{3.8}$$

and $\overline{F}(\omega)$ is the two-exciton Green function for excitons treated as noninteracting bosons:

$$\overline{F}(\omega)\equiv[(\omega+2i\eta)-(h_{12}+h_{34})]^{-1}. \tag{3.9}$$

Equations (3.3)–(3.9) provide closed formal expressions for $\chi^{(1)}$ and $\chi^{(3)}$ for a general two-band model. These GFE's were presented in Ref. 52 in a matrix (rather than operator) form. The GFE treats optical nonlinearities in terms of exciton-exciton scattering represented by $\overline{\Gamma}(\omega)$.

In many cases spin and real-space variables of electrons and holes can be treated separately, and a convenient representation is obtained by treating all operators in one- and two-exciton spaces as matrices in spin space and operators in real space. The GFE adopts the following form:

$$\chi^{(3)}(-\omega_s\mathbf{r}_s;\omega_1\mathbf{r}_1,\omega_2\mathbf{r}_2,-\omega_3\mathbf{r}_3) = \tfrac{1}{6}\sum_{perm}\sum_{\alpha_s\alpha_1\alpha_2\alpha_3}\langle\mu_{\alpha_s}(\mathbf{r}_s)\otimes\mu_{\alpha_3}(\mathbf{r}_3)| \times R_{\alpha_s\alpha_1\alpha_2\alpha_3}(-\omega_s;\omega_1,\omega_2,-\omega_3)|\mu_{\alpha_1}(\mathbf{r}_1)\otimes\mu_{\alpha_2}(\mathbf{r}_2)\rangle, \tag{3.10}$$

where Greek indices represent the spin variables of electron-hole pairs (excitons), and Σ_{perm} denotes a sum over the six permutations of $\omega_1\mathbf{r}_1\alpha_1$, $\omega_2\mathbf{r}_2\alpha_2$, and $-\omega_3\mathbf{r}_3\alpha_3$:

$$R_{\alpha_s\alpha_1\alpha_2\alpha_3}(-\omega_s;\omega_1,\omega_2,-\omega_3)=G(\omega_s)\otimes G^\dagger(\omega_3)\overline{\Gamma}_{\alpha_s\alpha_3,\alpha_1\alpha_2}(\omega_1+\omega_2)G(\omega_1)\otimes G(\omega_2), \tag{3.11}$$

where

$$\overline{\Gamma}_{\alpha\beta,\mu\nu}(\omega)=-2\overline{P}_{\alpha\beta,\mu\nu}P[\overline{F}(\omega)]^{-1} +2U(\omega-H+2i\eta)^{-1} \times(I\overline{I}_{\alpha\beta,\mu\nu}-P\overline{P}_{\alpha\beta,\mu\nu})[\overline{F}(\omega)]^{-1}, \tag{3.12}$$

$\overline{P}_{\alpha\beta,\mu\nu}$ are matrix elements of the electron angular momentum permutation, whereas $\overline{I}_{\alpha\beta,\mu\nu}$ are matrix elements of the unit operator in the angular-momentum two-exciton space, and

$$H \equiv h_{12} + h_{34} + U. \tag{3.13}$$

Equations (3.10)–(3.12) express $\chi^{(3)}$ in terms of operators acting only in real space, and provide general expressions for the frequency-domain third-order optical response of semiconductors. The two-exciton scattering matrix [Eq. (3.12)] has two terms. The first includes exciton-exciton scattering due to statistical properties, and the second reflects nonlinearities induced by the many-body Coulomb interaction. In the coming sections we will apply Eqs. (3.10)–(3.12) to calculate the frequency-domain third-order optical response of quantum wells in a strong magnetic field. We will also use Eqs. (3.1) and (3.2) to analyze the time-domain optical response of the same system.

IV. ONE- AND TWO-EXCITON STATES OF QUANTUM WELLS IN A STRONG MAGNETIC FIELD

Equations (3.10)–(3.13), which give $\chi^{(3)}$ for a general two-band model, require an extensive numerical effort since Eq. (3.12) for $\overline{\Gamma}(\omega)$ involves inverting of the operator $(\omega - H + 2i\eta)$in the two-exciton space. It is very difficult to solve a four-particle problem either analytically or numerically. However, in the case of semiconductor quantum wells in a strong magnetic field, the large separations between electron (or hole) Landau levels, together with the high symmetry of the problem, makes it possible to calculate one-exciton states analytically and to construct convenient basis sets in the space of relevant two-exciton states. This provides an efficient algorithm for computing $\chi^{(3)}$ as well as approximations for limiting cases.

We consider a two-dimensional semiconductor nanostructure, i.e., a thin quantum well, in the xy plane with a magnetic field H applied in the z direction. When H is strong, we can neglect the Coulomb coupling between excitons formed by electrons or holes from different Landau levels, and restrict the electron and hole to the lowest Landau levels (other Landau levels can be considered in a similar manner). In this section we start with a two-band Hamiltonian for a quantum well in strong magnetic field. We derive a two-band Hamiltonian which only incorporates those electrons (holes) belonging to the lowest electron (hole) Landau levels, We then calculate the one-exciton Hamiltonian h, the permutation operators P, and the exciton-exciton interaction operator U. These will allow to apply the GFE's [Eqs. (3.9)–(3.12)] for calculating $\chi^{(3)}$ of magnetoexcitons.

We assume that the kinetic-energy operators of electrons and holes possess two-dimensional Poincaré symmetry (i.e., with respect to translations and rotations), and the charge-density operator responsible for the Coulomb interactions between electrons and holes has a form

$$\rho(\mathbf{r}) = e[\hat{\Psi}_e^\dagger(\mathbf{r})\hat{\Psi}_e(\mathbf{r}) - \hat{\Psi}_h^\dagger(\mathbf{r})\hat{\Psi}_h(\mathbf{r})], \tag{4.1}$$

where $\hat{\Psi}_e(\mathbf{r})$ $[\hat{\Psi}_h(\mathbf{r})]$ is the annihilation operator for an electron (hole) at point $\mathbf{r}$. We further assume that interactions with the external transverse field conserve translational symmetry (since optical wave vectors are small compared to all other length scales in the problem).

The Hamiltonian $\mathcal{H}$ describing electrons and holes in a magnetic field is given by

$$\mathcal{H} = \sum_i H_i + \sum_{ij} H_{ij}, \tag{4.2}$$

with $i,j = e,h$ where H_e and H_h contain the kinetic energies including the terms induced by the magnetic fields for electrons and holes with effective masses m_e and m_h, respectively:

$$H_j = \int \hat{\Psi}_j^\dagger(\mathbf{r}) \frac{1}{2m_j} \left(\tilde{\mathbf{p}}_j + s_j \frac{e}{c} \mathbf{A}(\mathbf{r}) \right)^2 \hat{\Psi}_j(\mathbf{r}) d\mathbf{r}, \tag{4.3}$$

where $s_e \equiv 1, s_h \equiv -1$, and $\tilde{\mathbf{p}} \equiv -i\hbar\partial/\partial\mathbf{r}$. H_{ij} describe the Coulomb interaction, and are given by

$$H_{ij} = \frac{s_{ij}}{2} \int \hat{\Psi}_i^\dagger(\mathbf{r}) \hat{\Psi}_j^\dagger(\mathbf{r}') \frac{e^2}{\varepsilon_{ij}|\mathbf{r}-\mathbf{r}'|} \hat{\Psi}_j(\mathbf{r}') \hat{\Psi}_i(\mathbf{r}) d\mathbf{r} d\mathbf{r}', \tag{4.4}$$

where $s_{ee} = s_{hh} \equiv 1$, and $s_{eh} = s_{he} \equiv -1$.

The vector potential $\mathbf{A}(\mathbf{r})$ is chosen in the holomorphic gauge

$$\mathbf{A}(\mathbf{r}) \equiv \tfrac{1}{2}[\mathbf{r},\mathbf{H}], \tag{4.5}$$

where $\mathbf{H}$ represents homogeneous magnetic field in the z direction. Hereafter we will also use a notation $[\mathbf{r},\mathbf{H}] \equiv \mathbf{r} \times \mathbf{H}$ for the vector products. In Eq. (4.4), ε_{ij} are dielectric constants which determine the Coulomb potentials

$$V_{ij}(\mathbf{r},\mathbf{r}') \equiv \frac{e^2}{\varepsilon_{ij}(\mathbf{r}-\mathbf{r}')|\mathbf{r}-\mathbf{r}'|} s_{ij}. \tag{4.6}$$

These allow us to use different values of electron-electron, hole-hole, and electron-hole Coulomb interactions. Treating ε_{ij} as functions of $|\mathbf{r}-\mathbf{r}'|$ we can consider deviations of potentials from the $\sim|\mathbf{r}-\mathbf{r}'|^{-1}$ form, which are important at distances comparable to the transverse size of a quantum well or even at larger sizes in the case of superlattices. The reason is as follows: realistic quantum wells are not exactly two dimensional, but are characterized by a finite width in the transverse direction. A more rigorous three-dimensional calculation of these matrix elements should take into account the in-plane as well as the transverse confinement wave functions which may be different for electrons $[\Phi_e(\xi)]$ and holes and $[\Phi_h(\xi)]$. For small in-plane momenta, these confinement wave functions introduce a factor

$$\int \int \Phi_{i_1}^*(\xi) \Phi_{i_2}^*(\xi') \Phi_{i_3}(\xi') \Phi_{i_4}(\xi) d\xi\, d\xi' \tag{4.7}$$

into the Coulomb potential. For our system we have $i_j = e$, $j = 1$ and 4, for the electron-electron part of the interaction, $i_j = h$, $j = 1$, and 4, for the hole-hole part, and $i_1 = i_4 = e$ and $i_2 = i_3 = h$ for the electron-hole part (which also determines the single-exciton binding energy). This dependence of the Coulomb interaction on the confinement wave function introduces an asymmetry between the particle-particle and the

particle-hole part of the interaction, which has important signatures in two-exciton spectroscopy, as will be shown below. Another possible source of asymmetry may come from the single-particle dispersions, which especially for the holes may not be isotropic. However, this effect, and also the valence-band mixing effect,[16] are neglected in the following calculations, where we employ the effective mass model for both electrons and holes.

In our calculations we assumed the following forms for the Coulomb potentials;

$$V_{eh}(\mathbf{r},\mathbf{r}')=-\frac{\alpha}{|\mathbf{r}-\mathbf{r}'|}\{1+\kappa_{eh}\ \exp[-|\mathbf{r}-\mathbf{r}'|^2/r_0^2]\},$$

$$V_{ee}(\mathbf{r},\mathbf{r}')=V_{hh}(\mathbf{r},\mathbf{r}')$$

$$=\frac{\alpha}{|\mathbf{r}-\mathbf{r}'|}\{1+\kappa_{ee}\exp[-|\mathbf{r}-\mathbf{r}'|^2/r_0^2]\}. \quad (4.8)$$

This form may be rationalized as follows. At large distances the particle-particle and particle-hole potentials should behave like $\pm\alpha|\mathbf{r}-\mathbf{r}'|^{-1}$, and electron-hole asymmetry in the Coulomb interactions should vanish. This short-range asymmetry is modeled in Eqs. (4.8) by the Gaussian term. The asymmetry length-parameter r_0 is chosen to be the same for all potentials, whereas the parameters κ_{eh} and κ_{ee} represent its magnitude.

It is important to note that although the vector potential given by Eq. (4.5) is not translationally invariant, translational symmetry is not destroyed: it should be redefined by adding a phase vector (see Appendix A). The momentum operators no longer commute, and the Poincaré symmetry is transformed to its central extension, hereafter referred to as Poincaré-Weyl-Heisenberg (PWH) symmetry (see Appendix A for details). Classification of irreducible representations of the PWH algebra is given in Appendix B. Adopting this language, the electron and hole Landau levels can be treated as irreducible representations of the PWH algebra, which shows an algebraic origin of the energetic degeneracy of Landau levels.

Hereafter we switch to dimensionless coordinates r/l_H scaled by the characteristic magnetic length $l_H\equiv\sqrt{\hbar/eH}$. Using holomorphic coordinates z_e, and z_h for electrons and holes ($z=x+iy$) we obtain the electron and hole wave functions on the lowest Landau levels:

$$\psi(\mathbf{r}_e)=\varphi(\bar{z}_e)\exp\left[-\frac{|z_e|^2}{4}\right], \quad (4.9)$$

$$\psi(\mathbf{r}_h)=\varphi(z_h)\exp\left[-\frac{|z_h|^2}{4}\right], \quad (4.10)$$

where φ is an arbitrary function.

Using Eqs. (4.9) and (4.10) we can introduce basis sets in the one-electron and one-hole spaces corresponding to the lowest Landau level.

$$\varphi_{m_1}(\mathbf{r}_e)=\frac{1}{\sqrt{\pi}2^{m_1+1}\sqrt{m_1!}}\bar{z}_e^{m_1}\exp\left[-\frac{|z_e|^2}{4}\right], \quad (4.11)$$

$$\varphi_{m_2}(\mathbf{r}_h)=\frac{1}{\sqrt{\pi}2^{m_2+1}\sqrt{m_2!}}z_h^{m_2}\exp\left[-\frac{|z_h|^2}{4}\right]. \quad (4.12)$$

Considering electrons and holes which belong to the lowest Landau level and making use of Eqs. (4.11) and (4.12), we represent the field operators $\hat{\Psi}_j(\mathbf{r})$ in forms

$$\hat{\Psi}_e(\mathbf{r})=\sum_{m_1=0}^{\infty}\frac{1}{\sqrt{\pi}2^{m_1+1}\sqrt{m_1!}}\bar{z}^{m_1}\exp\left[-\frac{|z|^2}{4}\right]a_{m_1}, \quad (4.13)$$

$$\hat{\Psi}_h(\mathbf{r})=\sum_{m_2=0}^{\infty}\frac{1}{\sqrt{\pi}2^{m_2+1}\sqrt{m_2!}}z^{m_2}\exp\left[-\frac{|z|^2}{4}\right]b_{m_2}, \quad (4.14)$$

where a_{m_1} (b_{m_2}) are electron (hole) annihilation operators introduced in Sec. II for the general two-band model.

Substituting Eqs. (4.13) and (4.14) into Eqs. (4.2)–(4.4), we recast the two-band Hamiltonian in the form of Eq. (2.1), where indices m_1 (m_2) represent electron (hole) states on the lowest Landau level. The parameters of the Hamiltonian $V^{(j)}$ and W are expressed in terms of integrals involving Coulomb potentials and wave functions [Eqs. (4.11) and (4.12)]. For $t^{(j)}$ we have

$$t^{(e)}_{m_1n_1}=E_0^{(e)}\delta_{m_1n_1},\quad t^{(h)}_{m_2n_2}=E_0^{(h)}\delta_{m_2n_2} \quad (4.15)$$

where $E_0^{(e)}[E_0^{(h)}]$ is the electron (hole) energy on the lowest Landau level.

To calculate the matrix elements of operators h, U, and P, we start with h, which operates in the space of one-exciton (one electron and one hole) states. According to Eqs. (4.9) and (4.10), a state with one electron and one hole can be represented as

$$\Psi(\mathbf{r}_e,\mathbf{r}_h)=\varphi(\bar{z}_e,z_h)\exp\left[-\frac{|z_e|^2}{4}-\frac{|z_h|^2}{4}\right]. \quad (4.16)$$

Since the total charge of an excitonic state is zero $[\hat{p}_1,\hat{p}_2]=0$ wave functions with given center-of-mass momenta $\mathbf{p}$ form a basis set of eigenstates of the Hamiltonian h in the space of functions given by Eq. (4.16), a normalized wave function with momentum $\mathbf{p}$ can be easily found and has a form

$$\Psi^{(1)}_{\mathbf{p}}(\mathbf{r}_e,\mathbf{r}_h)=\frac{1}{(2\pi)^{3/2}}\exp\left[-\frac{p^2}{4}\right]\exp\left\{-\frac{r^2}{4}+\frac{i}{2}\mathbf{n}\cdot[\mathbf{r},\mathbf{R}]\right.$$

$$\left.+i\mathbf{p}\cdot\mathbf{R}+\frac{1}{2}\mathbf{n}\cdot[\mathbf{p},\mathbf{r}]\right\}, \quad (4.17)$$

where $\mathbf{R}=\frac{1}{2}(\mathbf{r}_e+\mathbf{r}_h)$, $\mathbf{r}=\mathbf{r}_e-\mathbf{r}_h$, and $\mathbf{n}$ is a unit vector in the z direction.

Hereafter we use the basis set $\Psi_{\mathbf{p}}$ represented by Eq. (4.17) in the one-exciton space instead of the basis set $m=(m_1m_2)$. Due to translational symmetry, the operator h is diagonal in the $\Psi_{\mathbf{p}}$ basis set. Its eigenvalues $\epsilon_{\mathbf{p}}$ may be obtained by evaluating the expectation values of the operator h given by Eq. (2.10) using one-exciton wave functions given by Eq. (4.17). A direct calculation yields

$$\epsilon_{\mathbf{p}}=E_0-\alpha\sqrt{\frac{\pi}{2}}\left\{\left(I_0\left(\frac{p^2}{4}\right)\exp\left[-\frac{p^2}{4}\right]+\kappa_{eh}\frac{1}{\sqrt{1+2/r_0^2}}I_0\left(\frac{p^2}{4(1+2/r_0^2)}\right)\exp\left[-\frac{p^2}{4}\left(\frac{1+4/r_0^2}{1+2/r_0^2}\right)\right]\right\}\right. . \tag{4.18}$$

Here α is the constant of the Coulomb interaction written in dimensionless units of length, I_0 is the modified Bessel function, and $E_0\equiv E_0^{(e)}+E_0^{(h)}$ is the sum of Landau energies of an electron and a hole.

We next turn to the operators P and U acting in the two-exciton space. It is not necessary to calculate matrix elements of these operators between all two-exciton states since only two-exciton states with zero total momentum and angular momentum are involved in the optical response. Hereafter we refer to them as the relevant two-exciton states. (Using more formal language the relevant states are those which are symmetric with respect to the PWH algebra.) This allows us to use the theory of representations to find convenient basis sets in the space of relevant two-exciton states. If V_0 is the PHW algebra representation related to the lowest electron Landau level (see Appendixes A and B), then V_0^* (the dual representation) is related to the lowest hole level. The space of one-exciton states is $V_0\otimes V_0^*$, and the space of two-exciton states is $W\equiv(V_0\otimes V_0^*)\otimes(V_0\otimes V_0^*)$.

Since we are interested only in zero-momentum two-exciton states, we need to decompose W into a sum of irreducible representations and keep only unit components (i.e., one-dimensional representations of the vectors which are not affected by the action of the algebra). This can be done in two ways leading to two convenient basis sets (see Appendix C). A discrete basis set is obtained by representing $W=(V_0\otimes V_0)\otimes(V_0^*\otimes V_0^*)$, decomposing $V_0\otimes V_0$ and $V_0^*\otimes V_0^*$ into a direct sum of irreducible representations and by finding the symmetric components in the product $(V_0\otimes V_0)\otimes(V_0^*\otimes V_0^*)$. This leads to a basis set represented by two-exciton wave functions Ψ_n given by Eq. (C7). The matrix elements U_{mn} and H_{mn} of the operators U [Eq. (2.11)] and H [Eq. (3.13)] are evaluated and given in Appendixes C and D. The matrix elements of P have the form (see Appendix C)

$$P_{mn}=(-1)^m\delta_{mn}. \tag{4.19}$$

An alternative, continuous, basis set is obtained by representing $W=(V_0\otimes V_0^*)\otimes(V_0\otimes V_0^*)$. As shown before, one-exciton wave functions $\Psi_{\mathbf{p}}^{(1)}$ [Eq. (4.17)] form a basis set in $V_0\otimes V_0^*$. Translationally invariant two-exciton wavefunctions are represented by $\psi_{\mathbf{p}}$ defined by

$$\psi_{\mathbf{p}}\equiv\psi_{\mathbf{p}}^{(1)}\otimes\psi_{-\mathbf{p}}^{(1)}. \tag{4.20}$$

The relevant two-exciton states which are translationally invariant as well as have zero angular momentum can be obtained by

$$\psi_q^{(2)}\equiv\int d\mathbf{p}\ \delta(|\mathbf{p}|-q)\,\psi_{\mathbf{p}}; \tag{4.21}$$

however, it is more convenient to work in a larger space represented by $\psi_{\mathbf{p}}$.

The matrix elements $U_{\mathbf{pp}'}$, $H_{\mathbf{qq}'}$, and $P_{\mathbf{qq}'}$ are evaluated in Appendix E, yielding

$$P_{\mathbf{pp}'}=\frac{1}{4\pi}(e^{-i\mathbf{n}\cdot[\mathbf{p},\mathbf{p}']}+e^{i\mathbf{n}\cdot[\mathbf{p},\mathbf{p}']}) \tag{4.22}$$

which implies that in the continuous basis set P acts as a Fourier transform. The matrix elements $U_{\mathbf{pp}'}$ and $H_{\mathbf{qq}'}$ are given in Appendix E.

In summary, we found the eigenstates of the one-exciton Hamiltonian h, and matrix elements of the operators U and H using two basis sets in the space of relevant two-exciton states. In Sec. V we combine these results with the GFE for $\chi^{(3)}$ obtained in Sec. III to derive a closed expression for the third-order susceptibility of quantum wells in a strong magnetic field.

V. THIRD-ORDER SUSCEPTIBILITY OF MAGNETOEXCITONS

We start our derivation by switching to the momentum (k) space. Introducing

$$\mu_\alpha(\mathbf{k})\equiv\int d\mathbf{r}\ e^{-i\mathbf{k}\cdot\mathbf{r}}\mu_\alpha(\mathbf{r}), \tag{5.1}$$

we obtain

$$\begin{aligned}\chi^{(3)}&(-\omega_s-\mathbf{k}_s;\omega_1\mathbf{k}_1,\omega_2\mathbf{k}_2,-\omega_3-\mathbf{k}_3)\\&=\tfrac{1}{6}\sum_{perm}\sum_{\alpha_s\alpha_1\alpha_2\alpha_3}\langle\mu_{\alpha_s}(\mathbf{k}_s)\otimes\mu_{\alpha_3}(\mathbf{k}_3)|\\&\quad\times R_{\alpha_s\alpha_1\alpha_2\alpha_3}(-\omega_s;\omega_1,\omega_2,-\omega_3)|\mu_{\alpha_1}(\mathbf{k}_1)\otimes\mu_{\alpha_2}(\mathbf{k}_2)\rangle.\end{aligned} \tag{5.2}$$

Substituting Eq. (3.11) into Eq. (5.2) yields

$$\begin{aligned}\chi^{(3)}&[-\omega_s-\mathbf{k}_s;\omega_1\mathbf{k}_1,\omega_2\mathbf{k}_2,-\omega_3-\mathbf{k}_3]\\&=\tfrac{1}{6}\sum_{perm}\sum_{\alpha_1\alpha_2\alpha_3}\mu_{\alpha_s}\mu_{\alpha_1}\mu_{\alpha_2}\mu_{\alpha_3}\\&\quad\times\frac{1}{\omega_1-\epsilon_{\mathbf{k}_1}+i\eta}\,\frac{1}{\omega_2-\epsilon_{\mathbf{k}_2}+i\eta}\\&\quad\times\frac{1}{\omega_3-\epsilon_{\mathbf{k}_3}-i\eta}\,\frac{1}{\omega_s-\epsilon_{\mathbf{k}_s}+i\eta}\\&\quad\times\overline{\Gamma}_{\alpha_s\alpha_3,\alpha_1\alpha_2}(\omega_1+\omega_2;\mathbf{k}_s,\mathbf{k}_3;\mathbf{k}_1,\mathbf{k}_2),\end{aligned} \tag{5.3}$$

where we used

$$\boldsymbol{\mu}_{\boldsymbol{\alpha}}(\mathbf{k})\otimes\mu_{\beta}(\mathbf{q})=\mu_{\alpha}\mu_{\beta}\phi(\mathbf{k},\mathbf{q}) \tag{5.4}$$

which follows from translational symmetry. Here μ_α are numbers and $\phi(\mathbf{k}_1,\mathbf{k}_2)\equiv\psi^{(1)}_{\mathbf{k}_1}\otimes\psi^{(1)}_{\mathbf{k}_2}$ denotes a two-exciton state represented by a direct product of two one-exciton states with momenta $\mathbf{k}_1$ and $\mathbf{k}_2$, μ_α is the dipole of the exciton with polarization α, $\epsilon_{\mathbf{k}}$ is the exciton energy given by Eq. (4.18), and

$$\begin{aligned}&\overline{\Gamma}_{\alpha_s\alpha_3,\alpha_1\alpha_2}(\omega;\mathbf{k}_s,\mathbf{k}_3;\mathbf{k}_1,\mathbf{k}_2)\\&\quad\equiv\langle\phi(\mathbf{k}_s,\mathbf{k}_3)|\overline{\Gamma}_{\alpha_s\alpha_3,\alpha_1\alpha_2}(\omega)|\phi(\mathbf{k}_1,\mathbf{k}_2)\rangle.\end{aligned} \tag{5.5}$$

To calculate $\overline{\Gamma}$ we note that $\phi(\mathbf{p},-\mathbf{p})=\Psi_{\mathbf{p}}$, the latter is defined by Eq. (E1). Since in the $\Psi_{\mathbf{p}}$ basis set the operator P acts as a Fourier transform, we have

$$\begin{aligned}&\langle\phi(\mathbf{p},-\mathbf{p})|P|\phi(\mathbf{p}',-\mathbf{p}')\rangle\\&\quad=\frac{1}{4\pi}(e^{-i\mathbf{n}\cdot[\mathbf{p},\mathbf{p}']}+e^{i\mathbf{n}\cdot[\mathbf{p},\mathbf{p}']}).\end{aligned} \tag{5.6}$$

The wave function $\phi(0,0)$ represents a two-exciton state with zero total and angular momentum. It can be expanded through the states Ψ_n given by Eq. (C7) [see Eqs. (C9)–(C11)],

$$\phi(0,0)=\frac{1}{\sqrt{\pi}}\sum_n\Psi_n, \tag{5.7}$$

whereas

$$P\Psi_n=(-1)^n\Psi_n. \tag{5.8}$$

Setting $\mathbf{k}_s=\mathbf{k}_3=\mathbf{k}_2=\mathbf{k}_1=0$ in the right-hand side of Eq. (5.5) and making use of Eqs. (5.5)–(5.8) we finally obtain

$$\begin{aligned}&\chi^{(3)}(-\omega_s-\mathbf{k}_s;\omega_1\mathbf{k}_1,\omega_2\mathbf{k}_2,-\omega_3-\mathbf{k}_3)\\&\quad=\tfrac{1}{6}\sum_{perm}\sum_{\alpha_s\alpha_1\alpha_2\alpha_3}\mu_{\alpha_s}\mu_{\alpha_1}\mu_{\alpha_2}\mu_{\alpha_3}\\&\qquad\times\frac{1}{\omega_1-\epsilon_{\mathbf{k}_1}+i\eta}\frac{1}{\omega_2-\epsilon_{\mathbf{k}_2}+i\eta}\frac{1}{\omega_3-\epsilon_{\mathbf{k}_3}-i\eta}\\&\qquad\times\frac{1}{\omega_s-\epsilon_{\mathbf{k}_s}+i\eta}\overline{\Gamma}_{\alpha_s\alpha_3,\alpha_1\alpha_2}(\omega_1+\omega_2),\end{aligned} \tag{5.9}$$

where

$$\overline{\Gamma}_{\alpha\beta,\mu\nu}(\omega)=\overline{\Gamma}^{(1)}_{\alpha\beta,\mu\nu}(\omega)+\overline{\Gamma}^{(2)}_{\alpha\beta,\mu\nu}(\omega), \tag{5.10}$$

with

$$\overline{\Gamma}^{(1)}_{\alpha\beta,\mu\nu}(\omega)=-\frac{1}{\pi}(\omega-2\epsilon_0+2i\eta)\overline{P}_{\alpha\beta,\mu\nu},$$

$$\begin{aligned}\overline{\Gamma}^{(2)}_{\alpha\beta,\mu\nu}(\omega)=&\frac{2}{\pi}(\omega-2\epsilon_0+2i\eta)\\&\times\sum_{mn}[U(\omega-H+2i\eta)^{-1}]_{mn}\\&\times[\overline{I}_{\alpha\beta,\mu\nu}-(-1)^n\overline{P}_{\alpha\beta,\mu\nu}].\end{aligned} \tag{5.11}$$

Equations (5.9)–(5.11) constitute our closed final expression for $\chi^{(3)}$.

Equations (5.11) expresses $\overline{\Gamma}^{(2)}(\omega)$ using the discrete basis set. A similar expression using the continuous basis set can be derived in a similar way, yielding

$$\begin{aligned}\overline{\Gamma}^{(2)}_{\alpha\beta,\mu\nu}(\omega)=&2(\omega-2\epsilon_0+2i\eta)\\&\times\int d\mathbf{q}d\mathbf{p}U_{0\mathbf{q}}[(\omega-H+2i\eta)^{-1}]_{\mathbf{qp}}\\&\times\left(\overline{I}_{\alpha\beta,\mu\nu}\delta_{\mathbf{p}0}+\frac{1}{2\pi}\overline{P}_{\alpha\beta,\mu\nu}\right).\end{aligned} \tag{5.12}$$

VI. TWO-EXCITON RESONANCES IN PUMP-PROBE SPECTROSCOPY

The expressions for $\chi^{(3)}$ derived in Sec. V [Eqs. (5.9)–(5.11)] represent the susceptibility in terms of the exciton-exciton scattering matrix $\overline{\Gamma}(\omega)$, which is given by a sum of two terms $\overline{\Gamma}^{(1)}(\omega)$ and $\overline{\Gamma}^{(2)}(\omega)$ [Eq. (5.10)]. $\overline{\Gamma}^{(1)}$ describes effects of phase-space filling (or, using a different terminology, nonboson exciton statistics). Exciton statistics is determined by exciton wave functions which do not depend on the exciton-exciton interaction operator U; $\overline{\Gamma}^{(1)}$ has therefore a universal U-independent form given by Eq. (5.11). $\overline{\Gamma}^{(2)}$ describes scattering induced by exciton-exciton interactions and vanishes for $U=0$. In this section $\overline{\Gamma}^{(2)}$ will be calculated numerically using Eq. (5.11). Analytical expressions for $\overline{\Gamma}^{(2)}$ for some limiting cases are presented in Appendix F.

It has been known since the early 1980s that if electron-electron, hole-hole, and electron-hole interactions have the same form [e.g., $\kappa_{ee}=\kappa_{eh}$ in Eq. (4.8)] and the bands are isotropic (this is known as the symmetric model), excitons do not interact at large distances, resembling the behavior of free bosons,[54] and the exciton-exciton scattering amplitude vanishes for small exciton momenta. Weak asymmetry ($\kappa_{ee}\neq\kappa_{eh}$) leads to the appearance of exciton-exciton elastic scattering with a universal behavior of the scattering amplitude $S(k)=(\sqrt{k}\ln k)^{-1}$ (Ref. 53) at small momenta, which strongly affects the thermodynamic properties of the exciton gas. Since the nonlinear optical response of harmonic systems is known to vanish,[37] $S(k)$ should have some direct signatures in $\chi^{(3)}$.

In order to calculate the optical response of this system we need to take into account the angular momenta of electrons and holes. As discussed in Ref. 30, the optical excitation of the energetically lowest exciton in bulk GaAs corresponds to the excitation of an electron from an effective angular momenta $J=\frac{3}{2}$ valence band to a $J=\frac{1}{2}$ conduction band. Since excitons are made of band states close to the Γ

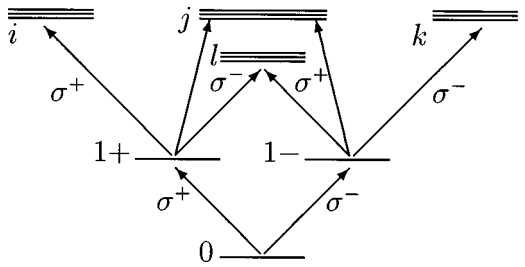

FIG. 2. Exciton level scheme for a GaAs quantum well. The two-exciton states are shown with indices i ($J=2, J_z=2$), j ($J=2, J_z=0$), k ($J=2, J_z=-2$), and l ($J=1, J_z=0$).

point $\mathbf{p}=0$, the conduction band can be described by a pair of $J_z=\pm\frac{1}{2}$ states and the valence band by pairs of $J_z=\pm\frac{3}{2}$ (heavy-hole) and $J_z=\pm\frac{1}{2}$ (light-hole) states. In a quantum well, the confinement lifts the degeneracy between the heavy-hole and light-hole excitons, and provides a natural quantization axis so that for fields polarized in the quantum-well plane only transitions with $\Delta J_z=\pm 1$ are dipole allowed. As displayed in Fig. 2, we neglect in the following the light holes and consider only the transitions between the heavy holes and the conduction-band, which gives rise to two degenerate single exciton resonances that can be excited by circularly polarized light σ^+ and σ^-, respectively.[30]

Since the eigenvalues of H_{mn} determine the resonances of $\overline{\Gamma}^{(2)}(\omega)$, we first examine the two-exciton states using H_{mn} [Eq. (C12)]. We call the eigenvalues of H_{mn} as ϵ_2 in the following. The variation of the two-exciton energies ϵ_2 with increasing dimensionality N_0 (N_0 is taken to be even) of the two-exciton matrix H_{ij} for $\kappa_{eh}=0$ and $\kappa_{ee}\geqslant 0$ is displayed in Figs. 3 and 4. We denote the one-exciton energy in a magnetic field H as $\Omega(H)$. The energy of two one-excitons Hamiltonians in the absence of a magnetic field $2\omega_0 \equiv 2\Omega(0)$ is taken to be zero. We use the GaAs parameters $m_e=0.0665$, $m_h=0.457$, and $\epsilon_0=13.74$.[2] Shown are calculations for three different asymmetry lengths $r_0/l_H=1$, 4, and 16, where the magnetic length $l_H=8.1$ nm for $H=10$ T.

Since $V^{(pp)}_{mn}$ is diagonal [see Eq. (C13)] and $V^{(eh)}_{mn}=0$ for $m+n=$odd [see Eq. (C15)] in the discrete basis set [Eq. (C7)], the two-exciton Hamiltonian H_{mn} is partitioned into two parts corresponding to both m and n being either even or odd. The two-exciton wave functions of H_{mn} for m,n even (odd) are symmetric (antisymmetric) with respect to the exchange of the two electrons and the two holes (without spin exchange). Figures 3 and 4 show the energies of symmetric and antisymmetric wave functions, respectively. There are no bound biexciton states in this case, since the particle-particle Coulomb interaction is stronger than particle-hole Coulomb interaction in exciton-exciton interaction. Figures 3(a) and 4(a) show that for symmetric Coulomb interaction the two-exciton energies change smoothly with increasing matrix dimensionality N_0, and form almost continuous levels between twice the one-exciton energy and the sum of the lowest Landau energy of two electrons and two holes for large N_0. Since the size of the two-exciton matrix is finite, we do not obtain a continuum. N_0 is related to the size of the quantum well in the xy direction: It gives the area of the quantum well, in units of l_H^2. The discrete energy levels appearing in the continuum reflect a finite-size effect.

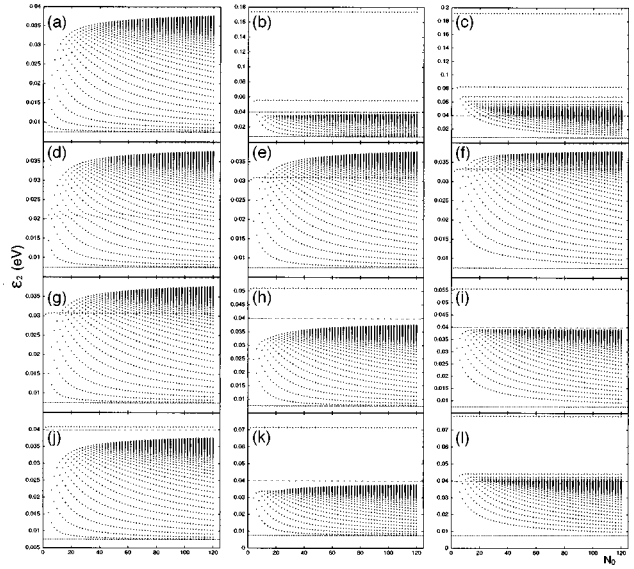

FIG. 3. Energies of the symmetric two-exciton eigenstates ϵ_2 for $\kappa_{eh}=0$ are displayed vs the dimensionality N_0 of the two-exciton matrix H_{mn}. [We denote the one-exciton energy in a magnetic field H as $\Omega(H)$.] The energy of two one-excitons in the absence of a magnetic field $2\omega_0 \equiv 2\Omega(0)$ is taken to be zero. Left, middle, and right columns represent $r_0=1$, 4, and 16, respectively. (a) $\kappa_{ee}=0$. (b) and (c) $\kappa_{ee}=8$. (d)–(f) $\kappa_{ee}=1$. (g)–(i) $\kappa_{ee}=2$. (j)–(l) $\kappa_{ee}=3$. Twice the one-exciton energy (7.5 meV) is shown by the long dashed line. The sum of the lowest Landau energy of two electrons and two holes (39.9 meV) is given by the short dashed line.

The two-exciton energies are slightly modified by introducing a small Coulomb asymmetry. For $\kappa_{ee}=1$ [Fig. 3(d)], we can see a symmetric eigenstate whose energy does not change with N_0. This means that there is an eigenstate of the symmetric wave function in the continuum for an infinitely large quantum well. The energy of this eigenstate is shifted to the blue for large r_0. This is because we have a larger asymmetry for larger r_0. This single level is also blueshifted with increasing κ_{ee} [Fig. 3(g)], and finally splits out from the

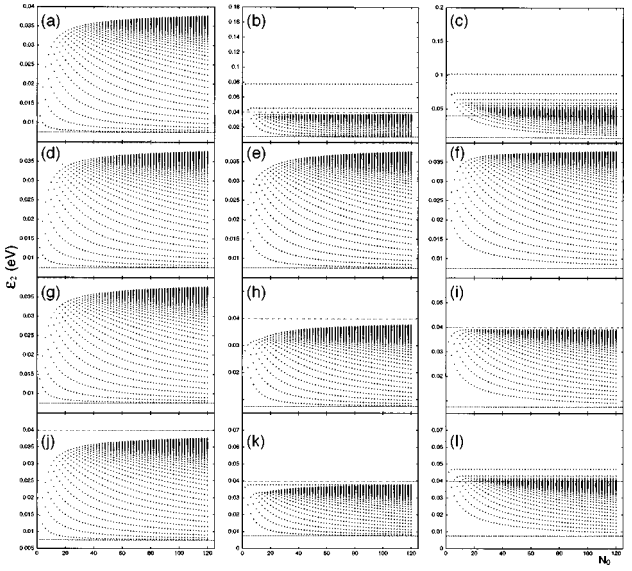

FIG. 4. Same as Fig. 3, but for the energies of antisymmetric two-exciton eigenstates.

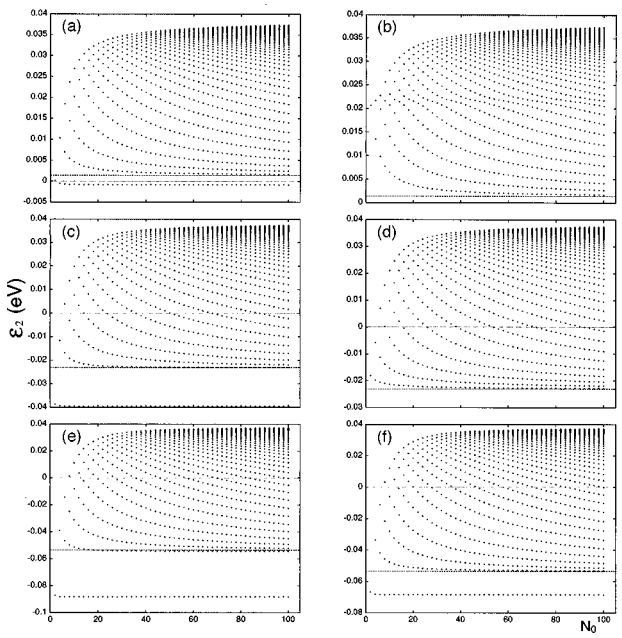

FIG. 5. Energies of the symmetric two exciton eigenstates same as Fig. 3 but for nonzero κ_{eh}. $r_0=4$. Left column: $\kappa_{ee}=0$; right column: $\kappa_{ee}=1$. (a) and (b) $\kappa_{eh}=0.2$. (c) and (d) $\kappa_{eh}=1$. (e) and (f) $\kappa_{eh}=2$. Twice the one-exciton energy is 1.4 meV [(a) and (b)], -23.0 meV [(c) and (d)], -53.6 meV [(e) and (f)].

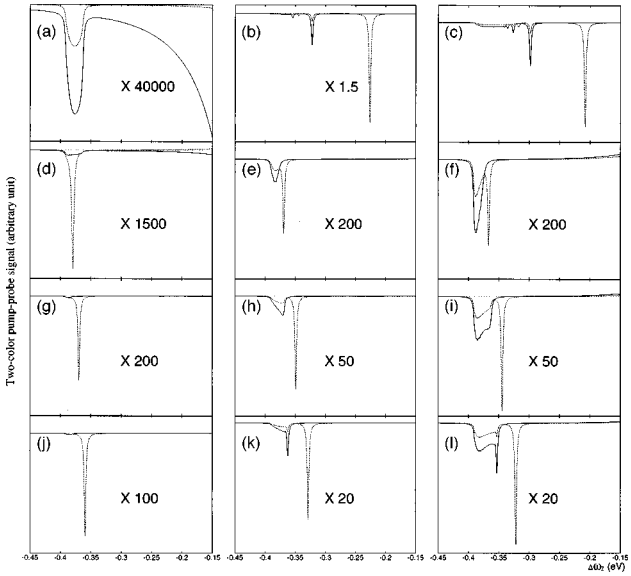

FIG. 7. The two-color pump-probe signal I_{pp} is displayed as a function of $\Delta\omega_2\equiv\omega_2-\omega_0$, with $\Delta\omega_1\equiv\omega_1-\omega_0=0.4$ eV fixed. $\eta=0.8$ meV, $N_0=100$. Solid line: both E_1 and E_2 have σ_+ polarization. Dashed line: E_1 is σ_+ polarized and E_2 is σ_- polarized. Left, middle, and right columns represent $r_0=1$, 4, and 16, respectively. (a) $\kappa_{ee}=0$. (b) and (c) $\kappa_{ee}=8$. (d)–(f) $\kappa_{ee}=1$. (g)–(i) $\kappa_{ee}=2$. (j)–(l) $\kappa_{ee}=3$.

continuum [Figs. 3(j), 3(h), and 3(i)]. For $\kappa_{ee}=3$ and $r_0=4$, we have also an antisymmetric eigenstate embedded in the continuum [Fig. 4(k)]. The larger the asymmetry, the larger is the number of discrete eigenvalues. Figures 3(b) and 4(c) show such an extreme case ($\kappa_{ee}=8$). The number of discrete eigenvalues is 5 (58) for $r_0=4$ ($r_0=16$).

Figures 5 and 6 show the energies of symmetric and antisymmetric wave functions of the two-exciton eigenstates, respectively. For $r_0=4$ and varying κ_{eh}, bound biexciton states are observed for $\kappa_{eh}>\kappa_{ee}$. Figures 5(a) and 6(a), which represent weak Coulomb asymmetry ($\kappa_{eh}=0.2$), show two bound biexciton states. For larger values of κ_{eh} the discrete part of the spectrum contains three bound biexciton states [Figs. 5(c) and 6(c) ($\kappa_{eh}=1$) and Figs. 5(e) and 6(e) ($\kappa_{eh}=2$)]. However, when κ_{eh} is increased further, the number of bound biexciton states does not increase significantly. This is because this number depends not only on κ_{eh} but also on r_0. For small r_0, the exciton-exciton attractive interaction rapidly becomes shallow at small distances, resulting in a small number of bound biexciton states. For larger r_0, the exciton-exciton attractive interaction can be strong enough to support many bound biexciton states.

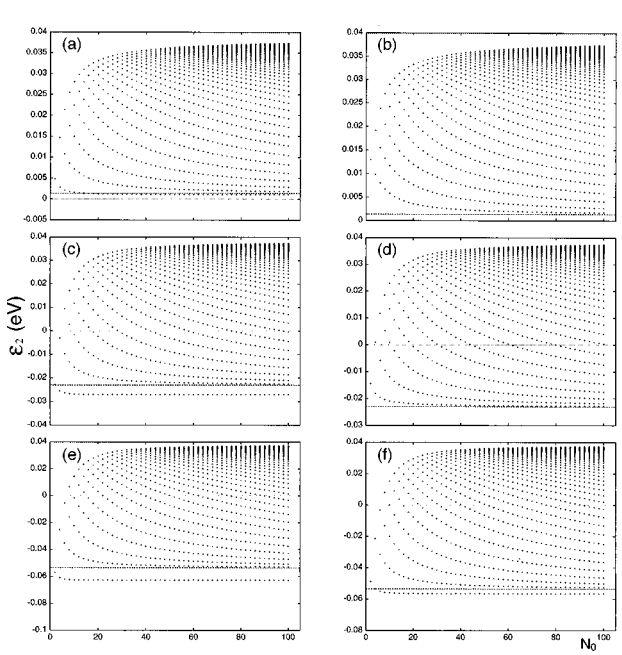

FIG. 6. Same as Fig. 5, but for the antisymmetric eigenstates.

For $\kappa_{ee}>\kappa_{eh}$, we expect a behavior similar to that displayed in Figs. 3 and 4. The spectrum displayed in Figs. 5(b) and 6(b) closely resembles that of Figs. 3(e) and 4(e). Figures 5(d) and 6(d) represent the symmetric Coulomb interaction [like Figs. 3(a) and 4(a)]. However, the nonlinear optical spectra are very different in this case, as will be demonstrated later in Fig. 8. Figures 5(f) and 6(f) are similar to Figs. 5 and 6, except for the number of bound biexciton states which is 2 and 3, respectively. This can be explained by the larger arguments in the former ($\kappa_{eh}=1$, $\kappa_{ee}=0$) compared with the latter ($\kappa_{eh}=2$, $\kappa_{ee}=1$).

We next turn to calculating $\chi^{(3)}$ using Eq. (5.9). $\bar{\Gamma}$ is evaluated using Eq. (3.12) utilizing the discrete basis set Ψ_n rather than Eqs. (5.10) and (5.11). The reason is the following: in deriving Eqs. (5.10) and (5.11) we invert $\bar{F}(\omega)$ in the full (infinite-dimensional) two-exciton space which yields $[\bar{F}(\omega)]^{-1}=\omega-2\epsilon_0+2i\eta$. However performing calculations in the N_0-dimensional subspace, $\bar{F}(\omega)$ should be inverted in the subspace in order not to miss some delicate cancellations.

The two-color pump-probe signal is given by

$$I_{pp}(\omega_2,\omega_1)=\mathrm{Im}\ \chi^{(3)}(-\omega_2;\omega_1,\omega_2,-\omega_1), \qquad (6.1)$$

where ω_1 (ω_2) represents the pump (probe) frequency. In Fig. 7 we display I_{pp} for different values of the asymmetry. In all cases we use $\omega_1-\omega_0=0.4$ eV, $\eta=0.8$ meV, and $H=10$ T, and tune ω_2 across the two-exciton band. The solid line represents the case when both fields have σ_+ polarization, whereas the dashed line corresponds to a σ_+ polarized pump and a σ_- polarized probe.

We have chosen ω_1 to be well above ω_0 to avoid interference between one- and two-exciton resonances and obtain the two-exciton resonances, in an unambigous way. Since in our model we consider only the lowest Landau level, it makes no difference whether $\omega_1-\omega_0$ is positive or negative. In a realistic system one needs to tune ω_1 carefully to avoid resonances with higher Landau levels and higher subbands which can lead to the creation of real excitations on higher levels, and affect the pump-probe signal because of relaxation. Another option is to choose ω_1 well below ω_0, where the structure of two-exciton resonances is the same as in the previous case.

Figure 7(a) shows that the signal for symmetric Coulomb interaction is considerably smaller compared to the asymmetric Coulomb interaction cases. This is consistent with the discussion given in Appendix F. The reason why we have small but finite signal for symmetric Coulomb interaction is that we used a finite-size two-exciton matrix which reflects the finite quantum-well size. We will return to this issue in Fig. 9. Since the signal is very weak, we can see the effect of one-exciton resonances in the blue part of the spectrum. In Figs. 7(d)–7(j) we clearly see a sharp peak which is blue shifted with increasing κ_{ee}. This peak corresponds to the eigenstate with symmetric wave function appearing in Figs. 3(d), 3(g), and 3(j). The solid line does not show a peak, since a symmetric wave function contributes to the signal only in the case of different polarizations of E_1 and E_2. We note a large broad peak which originates in the continuum part of the two-exciton levels. However this broad peak becomes almost negligible compared to the sharp discrete-level resonances for large asymmetry κ_{ee} [see Figs. 7(b) and 7(c)].

In Fig. 7(k) both signals show peaks at the top of the two-exciton band corresponding to the eigenstate inside the band shown in Fig. 4(k). Since this eigenstate has an antisymmetric wave function, it couples both cases where E_1 and E_2 have the same or different polarizations. For large κ_{ee} [Figs. 7(b) and 7(c)], we have sharp resonances originating from the discrete eigenstates located above the continuum. Scanning from blue to red, we first see a dashed line peak. Next we find a solid line peak and a dashed line peak at the same energy. After that, the dashed line peak and degenerate solid and dashed line peaks alternate. This means that the eigenstate with symmetric and with antisymmetric wave function appears alternately. (In particular the highest energy eigenvalue corresponds to the symmetric wave function.) This is consistent with Figs. 3 and 4.

For nonzero κ_{eh}, I_{pp} is markedly different from the $\kappa_{eh}=0$ case. Hereafter we set the asymmetry size $r_0=4$. The weak Coulomb asymmetry case is presented in Fig. 8(a) ($\kappa_{eh}=0.2$, $\kappa_{ee}=0$). The signal is slightly different from the symmetric Coulomb interaction case given in Fig. 7(a), and we can still see the finite-size effect from the continuum. We also see two peaks below the continuum corresponding to the bound biexciton states [Figs. 5(a) and 6(a)]. Note that we have an almost degenerate lowest state of the symmetric and antisymmetric wave functions, for symmetric Coulomb interaction [Figs. 3(a), 4(a), 5(d), and 6(d)]. These two levels split because of the asymmetry of the Coulomb interaction. The splitting becomes larger for increasing asymmetry of the Coulomb interaction. In Fig. 8(c) ($\kappa_{eh}=1$, $\kappa_{ee}=0$), we can clearly see the splitting of these states. The splitting is increased in Fig. 8(e) ($\kappa_{eh}=2$, $\kappa_{ee}=0$). The magnitude of the signal increases as well for larger asymmetry of Coulomb interaction, as already seen in Fig. 7. Another feature of the two-color pump-probe signal for nonzero κ_{eh} is a wide two-exciton band compared with the $\kappa_{eh}=0$ case. Since the one-exciton bandwidth for fixed r_0 depend on κ_{eh} only, this holds for the continuum part of the two-exciton band as well. This explains why the signal coming from the bound biexciton in Fig. 8(f) ($\kappa_{eh}=2$, $\kappa_{ee}=1$) resembles that of Fig. 8(c), whereas the signal of the continuum part in Fig. 8(f) is similar to that of Fig. 8(e).

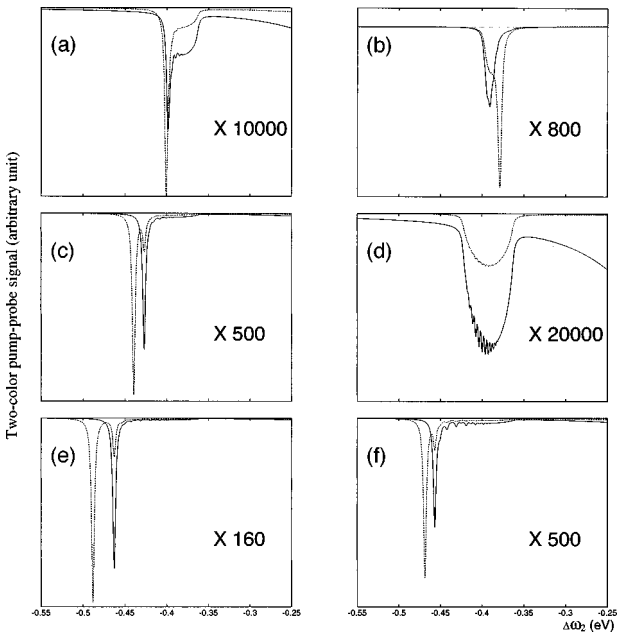

FIG. 8. Same as Fig. 7 but for nonzero κ_{eh}. $r_0=4$. Left column: $\kappa_{ee}=0$; right column: $\kappa_{ee}=1$. (a) and (b) $\kappa_{eh}=0.2$. (c) and (d) $\kappa_{eh}=1$. (e) and (f) $\kappa_{eh}=2$. Twice the one-exciton energy minus $2\omega_0$ is 1.4 meV [(a) and (b)], -23.0 meV [(c) and (d)], -53.6 meV [(e) and (f)].

Figure 8(b) ($\kappa_{eh}=0.2$, $\kappa_{ee}=1$) looks similar to Fig. 7(e). However, because of the reduced asymmetry coming from $\kappa_{eh}=0.2$, the magnitude of the signal in Fig. 8(b) is smaller.

Although both Figs. 7(a) and 8(d) represent symmetric Coulomb interaction, the signals show some differences. In Fig. 7(a) the continuum part of the spectrum is smooth, whereas the signal shown in Fig. 8(d) has some structure. (If we increase the phenomenological dephasing, these structure disappear, and the signal becomes smooth.) The reason for the observed structure in Fig. 8(d), in spite of the fact that we have used the same damping in both cases, is as follows: since $\kappa_{eh}=1$ in Fig. 8(d), the energy range of the continuum part is much wider than Fig. 7(a) ($\kappa_{eh}=0$). Consequently, if we do not add a large dephasing, we can see

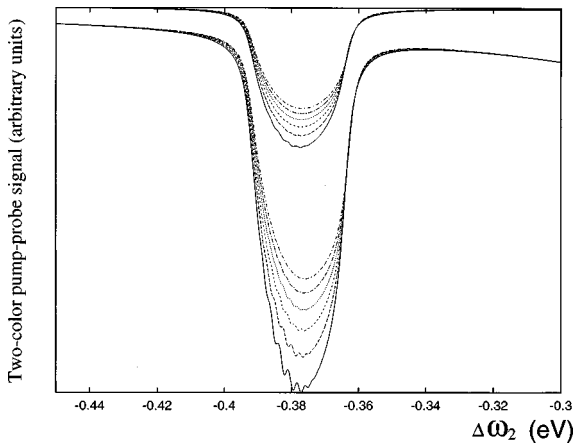

FIG. 9. Same as Fig. 8 but for various dimensionalities N_0 of the two-exciton matrix and symmetric Coulomb interaction ($\kappa_{ee}=\kappa_{eh}=0$). Upper six lines [$E_1$ (σ_+) and E_2 (σ_-) N_0] from bottom to top: 50, 60, 70, 80, 90, and 100. Lower six lines [E_1 $\sigma(_-)$ and E_2 (σ_-) N_0] from bottom to top: 50, 60, 70, 80, 90, and 100.

each peak which comes from the finite size effect. Another difference is that the height of the peak in Fig. 8(d) is about twice that of Fig. 7(a). This is explained by considering the fact that U in the case of $\kappa_{eh}=\kappa_{ee}=1$ is almost twice that of $\kappa_{eh}=\kappa_{ee}=0$ for $|\mathbf{r}-\mathbf{r}'|\ll r_0$ in Eq. (4.8).

Because of the slow convergence of the two-exciton levels of the continuum part with increasing N_0, the continuum part of the signal strongly depends on N_0. Figure 9 shows the two-color pump-probe signal for symmetric Coulomb interaction ($\kappa_{ee}=\kappa_{eh}=0$) for various dimensions of the two exciton matrix N_0. The signal at $\Delta\omega_2=0$ becomes smaller with increasing N_0. The peak height approximately shows the $\propto N_0^{-1/2}$ scaling. Therefore the value of the signal at $\Delta\omega_2=0$ vanishes for an infinitely large quantum well. In Appendix F, we show how $\chi^{(3)}$ for infinite systems is given by its LFA part, and, therefore, vanishes at $\Delta\omega_2=0$. Our numerical results are consistent with Appendix F.

The symmetric wave functions of the three lowest two-exciton eigenstates in the discrete basis Ψ_n in Eq. (C7) are displayed as a function of n of Ψ_n (x-axis) in Fig. 10. Since the two-exciton Hamiltonian (3.13) is decoupled into two parts, we have only $N_0/2$ nonzero components (x axis) for either symmetric or antisymmetric wave function (for even N_0). In order to obtain the wave functions, we used $N_0=100$ for the top panel and $N_0=120$ for the middle and bottom panels. For each panel the number of nodes increases with increasing two-exciton energy.

The eigenstates in Figs. 10(b) and 10(c) belong to the continuum part. From these panels we can see the slow convergence of the wave function with increasing N_0. For example, the lowest wave function does not have a node and does not go to zero for large n. Upon increasing the matrix size, the wave function becomes flatter and extends to large n. On the other hand, the wave functions in Fig. 10(a), which correspond to the bound biexcitons, converge. A small value of n dominates the wave functions of the lowest two eigenstates, and these wave functions rapidly vanish for large n. Even if we increase the size of the two-exciton matrix, these wave functions do not change appreciably. In Fig. 10(b) we have zero amplitude for small n. This is explained as follows: for $\kappa_{eh}<\kappa_{ee}$ the particle-particle Coulomb repulsive interaction is significantly stronger than the electron-hole Coulomb attractive interaction for $|\mathbf{r}-\mathbf{r}'|\ll r_0$ in Eq. (4.8). Here $|\mathbf{r}-\mathbf{r}'|\ll r_0$ is dominant for small n. As a result, we need to have a smaller amplitude for small n for the lowest eigenstate. The wave function of the lowest eigenstate in Fig. 10(a) is peaked at small n, since for $\kappa_{eh}>\kappa_{ee}$ the electron-hole Coulomb attractive interaction is significantly larger than the particle-particle Coulomb repulsive interaction for $|\mathbf{r}-\mathbf{r}'|\ll r_0$.

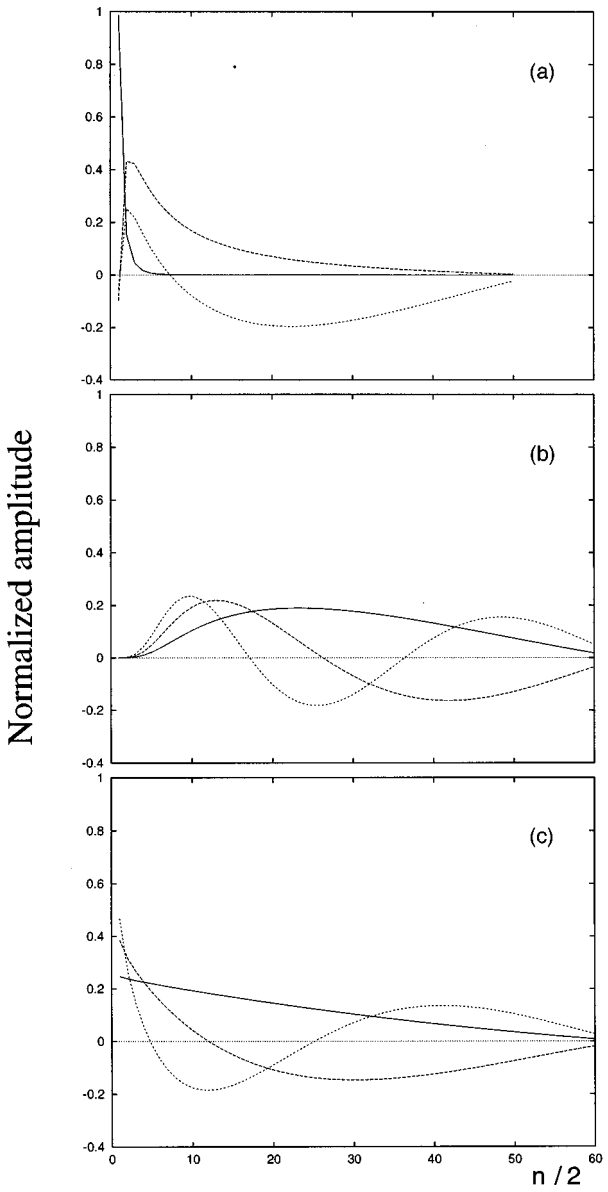

FIG. 10. The wave function of the three lowest symmetric two-exciton eigenstates in the discrete basis (x axis). (a) $\kappa_{eh}=2$, $\kappa_{ee}=0$. (b) $\kappa_{eh}=0$, $\kappa_{ee}=8$. (c) $\kappa_{ee}=\kappa_{eh}=0$. Solid line: the lowest two-exciton eigenstates. Long dashed line: the second lowest two-exciton eigenstates. Short dashed line: the third lowest two-exciton eigenstates. Note that the number of nodes increases with increasing two-exciton energy.

VII. SUMMARY

We have derived the GFE for the third order optical response of semiconductor systems by mapping the two-band

Hamiltonian onto an effective Frenkel exciton Hamiltonian. The GFE's express $\chi^{(3)}$ in the form of a product of four one-exciton Green functions and the exciton-exciton scattering matrix $\overline{\Gamma}$. The latter consists of two components which have a simple physical meaning: $\overline{\Gamma}^{(1)}$ represents the exciton-exciton scattering due to statistical properties of electron-hole pairs (phase filling), whereas $\overline{\Gamma}^{(2)}$ originates from the Coulomb interaction. We have applied the GFE's to calculate the pump-probe signals from GaAs quantum well in a strong magnetic field. Here we make use of the fact that in the limit of strong magnetic fields we can restrict the calculation to the lowest Landau-level exciton. The high symmetry of the system allows us to treat the relevant two-exciton states with a little computational effort. The role of asymmetry between the particle-particle and particle-hole interactions in optical nonlinearities was examined. We have shown that in the symmetric case (i.e., when the particle-particle and particle-hole interactions have the same magnitude) optical nonlinearities originate from effects of phase filling, and the exact analytical expression for $\chi^{(3)}$ has been derived. The asymmetry between particle-particle and particle-hole Coulomb interactions, which appears due to the fact that we study a pseudo-two-dimensional problem in a two-dimensional scheme, is determined by the asymmetry length r_0, which is related to the length scale on which the asymmetry occurs and the magnitudes of the deviation of the particle-particle and particle-hole interaction from the simple Coulomb law at distances shorter than r_0, denoted by κ_{ee} and κ_{eh}, respectively. The two-exciton wave functions are classified into two types, symmetric and antisymmetric, with respect to the exchange of the two electrons and two holes (without spin exchange). These correspond to total angular momentum $J=0$ and 2 states, respectively. The form of the pump-probe signals depends crucially on the asymmetry of the Coulomb interaction. We found a small but finite signal for the symmetric case ($\kappa_{eh}=\kappa_{ee}$), which is attributed to the finite size of the quantum well in the xy direction. For $\kappa_{eh}<\kappa_{ee}$ and small values of asymmetry, a well-defined discrete resonance appears inside the continuum. This resonance is blueshifted with increasing κ_{ee}, and splits out from the continuum at a certain value of κ_{ee}. The number of the discrete-level resonances for large asymmetry ($\kappa_{eh}\ll\kappa_{ee}$ and $1\ll\kappa_{ee}$) depends crucially on r_0. For $\kappa_{eh}>\kappa_{ee}$ the signal is dominated by bound biexcitons. The results presented in this paper are general for two-dimensional semiconductors in a strong perpendicular magnetic field. We expect that the predicted results should be found experimentally.

It should be emphasized that in the symmetric case the optical nonlinearity does not vanish: in this case the response is represented by that of an effective harmonic oscillator which is nonlinearly driven by the optical field. In this language, effects of phase space filling show up as nonlinear terms in the expansion of the polarization operator in powers of the effective oscillator coordinate. This implies that, in the symmetric case, $\chi^{(3)}$ vanishes at $\Delta\omega_2=0$. Under these conditions the main contribution to the optical nonlinearity will originate due to transitions between different Landau levels. These effects are not considered in the present paper since our goal is to study the structure of two-exciton resonances, and for resonant measurements in the asymmetric case the principal contribution comes from processes involving a single Landau level, provided the magnetic field is sufficiently strong.

Finally we note that a four-particle problem in a strong magnetic field has been considered in the context of the fractional quantum Hall problem, where the four particles are represented by a single hole with the charge e and three particles with the charge $-e/3$.[60] For that problem the constraints due to the symmetry are even stronger than in our case since there is only one hole in the complex, and $\chi^{(3)}$ can be found analytically.

ACKNOWLEDGMENTS

The support of the Air Force Office of Scientific Research, and the National Science Foundation, are gratefully acknowledged.

APPENDIX A: PARTICLES IN A HOMOGENEOUS MAGNETIC FIELD AND THE POINCARÉ-HEISENBERG-WEYL SYMMETRY

In the absence of a magnetic field the system has a symmetry with respect to the two-dimensional Poincaré algebra, which consists of translations

$$\hat{p}\equiv i\partial_m, \tag{A1}$$

where $\partial_m\equiv\partial/\partial r_m$, and rotations

$$\hat{M}\equiv -i\epsilon_{mn}r_m\partial_n, \tag{A2}$$

where ϵ_{mn} is the two-dimensional Levi-Cevita tensor and we assume summations over repeating indices. A homogeneous magnetic field in the z direction with the strength H can be described by a vector potential

$$A_m\equiv -\frac{H}{2}\epsilon_{mn}r_n, \tag{A3}$$

with $H=\epsilon_{mn}\partial_m A_n$. To take into account the magnetic field, we introduce the ''long'' derivative:

$$\nabla_m=\partial_m-ieA_m=\partial_m+i\frac{eH}{2}\epsilon_{mn}r_n, \tag{A4}$$

and substitute ∇_m instead of ∂_m everywhere in the Hamiltonian. Now we need to redefine the symmetry. Since rotations do not change, not only the magnetic field but the vector potential of Eq. (A3) as well, the operator $\hat{M}$ from Eq. (A2) commutes with the Hamiltonian in the presence of a magnetic field. Translations, conserving the magnetic field, change the vector potential. However, since the magnetic field is conserved, the shifted value of A differs from its original value by a gauge transformation. This implies that, to obtain operators of translations which commute with the Hamiltonian, a usual shift (translation) of a wave function should be accompanied by multiplication by $\exp[i\varphi(x)]$ to compensate for the change of A; i.e.,

$$T_a\Psi(x)=\exp[ie\varphi_a(x)]\Psi(x+a), \tag{A5}$$

with

$$A_m(x+a)-A_m(x)=\partial_m\varphi_a(x). \tag{A6}$$

A straightforward calculation making use of Eqs. (A5), (A6), and (A3) yields the following expressions for infinitesimal translations D_m:

$$D_m=\partial_m-i\frac{eH}{2}\epsilon_{mn}r_n. \tag{A7}$$

Naturally, we have

$$[D_m,\nabla_n]=0. \tag{A8}$$

We also obtain that the operators of translations D_m do not commute:

$$[D_m,D_n]=ieH\epsilon_{mn}. \tag{A9}$$

This is a consequence of the fact that, in the presence of the magnetic field, we have a projective representation of the Poincaré group:

$$T_aT_b\Psi=\exp[-i\varphi_{ab}]T_{a+b}\Psi, \tag{A10}$$

which originates from the fact that the function $\varphi_a(x)$ in Eq. (A5) is defined up to a constant [see Eq. (A6)]. According to a well-known theorem of the theory of representations,[59] each projective representation of a group can be considered as a usual representation of a central extension of the group which leads to the appearance of nonzero commutators like in Eq. (A9). Introducing the operators

$$\hat{p}_m\equiv -iD_m,\quad \hat{Q}\equiv eH, \tag{A11}$$

we obtain the Lie algebra generated by $\hat{p}_m$, $\hat{M}$, and $\hat{Q}$ with the following nonzero commutations

$$[\hat{p}_m,\hat{p}_n]=i\epsilon_{mn}\hat{Q},\quad [\hat{M},\hat{p}_m]=i\epsilon_{mn}\hat{p}_n, \tag{A12}$$

which forms a central extension of the Poincaré algebra (generated by $\hat{p}_m$ and $\hat{M}$ with the only nonzero commutations $[\hat{M},\hat{p}_m]=i\epsilon_{mn}\hat{p}_n$, $\hat{Q}$ being the central charge operator. We will refer to this as the PHW (Poincaré-Heisenberg-Weyl) algebra. The PHW algebra can be also treated as the algebra of a harmonic oscillator with $\hat{p}_1$, $\hat{p}_2$, and $\hat{M}$ being the momentum, coordinate, and Hamiltonian, respectively, and eH being the Planck constant. Expanding the action of the PHW algebra to multiparticle states, we obtain the central charge to be eH, where e is the total charge. This implies that, in the zero charge sector (i.e., the same number of electrons and holes), $\hat{Q}=0$, $[\hat{p}_1,\hat{p}_2]=0$, and one can define the momentum of a state.

Splitting of the space of single-particle states into Landau levels in the language of theory of representations means a decomposition of the representation of the PHW algebra in functions $\Psi(\mathbf{r})$ into a direct sum of irreducible representations V_n, where V_n is formed by all states which belong to the nth Landau level. The relation $\hat{H}\Psi=E_n\Psi$ for any $\Psi\in V_n$ follows from the fact that V_n's are irreducible, and $V_m\neq V_n$ for $m\neq n$.

APPENDIX B: CLASSIFICATION OF UNITARY REPRESENTATIONS OF THE PHW ALGEBRA

Here we present the classification of unitary representations of the PHW algebra; we will use it in the following sections to determine one- and two-exciton states. The first parameter of a representation is the central charge q; i.e., $\hat{Q}=q\hat{I}$ on the representation (where $\hat{I}$ is the unit operator).

(i) $q=0$. We then have irreducible representations parametrized by $p_0\geqslant 0$. The space of the representation is given by functions with the absolute value of momentum being p_0; i.e.,

$$\Psi(\mathbf{r})=\int d^2p\,\delta(|\mathbf{p}|-p_0)\,\gamma(\mathbf{p})\exp[i\mathbf{p}\cdot\mathbf{r}]: \tag{B1}$$

for $p_0>0$ a representation is infinite-dimensional; for $p_0=0$ it is a one-dimensional unit representation.

(ii) $q>0$. Each representation is determined by q and integer m, which is defined as follows: Let $|\Omega\rangle$ be the state which satisfies $(\hat{p}_1-i\hat{p}_2)|\Omega\rangle=0$, then $\hat{M}|\Omega\rangle=m|\Omega\rangle$.

(iii) $q<0$. m is defined by $(\hat{p}_1+i\hat{p}_2)|\Omega\rangle=0$ and $\hat{M}|\Omega\rangle=m|\Omega\rangle$. Using this language, the nth electron Landau level is given by the representation with $q=-|eH|$, $m=n$, and the nth hole Landau level by $q=|eH|$, $m=-n$. These representations are dual to each other.

APPENDIX C: BASIS SET FOR TWO-EXCITON STATES

We first represent

$$W\equiv(V_0\otimes V_0)\otimes(V_0^*\otimes V_0^*), \tag{C1}$$

and decompose

$$V_0\otimes V_0=\oplus_{n=0}^{\infty}V^{(n)},\quad V_0^*\otimes V_0^*=\oplus_{n=0}^{\infty}V^{(n)*}, \tag{C2}$$

where the orthonormal basis sets of irreducible representations $V^{(n)}$ and $V^{(n)*}$ are given by

$$(\Psi_n^{(e)})_m\equiv\frac{2^{-(m+n)}}{2\pi\sqrt{n!m!}}(\overline{z_1}-\overline{z_2})^n(\overline{z_1}+\overline{z_2})^m \times\exp\left[-\frac{|z_1|^2}{4}-\frac{|z_2|^2}{4}\right], \tag{C3}$$

$$(\Psi_n^{(h)})_m\equiv\frac{2^{-(m+n)}}{2\pi\sqrt{n!m!}}(w_1-w_2)^n(w_1+w_2)^m \times\exp\left[-\frac{|w_1|^2}{4}-\frac{|w_2|^2}{4}\right], \tag{C4}$$

where $(\Psi_n^{(e)})_m$ is the mth component of $\Psi_n^{(e)}$, and $m=0,1,2,\ldots$. Now we have

$$W=\oplus_{m,n=0}^{\infty}V^{(m)}\otimes V^{(n)*}. \tag{C5}$$

The unit representations is contained only in the terms with $m=n$, i.e., $V^{(n)}\otimes V^{(n)*}$, and each $V^{(n)}\otimes V^{(n)*}$ contains the unit representation only once;[59] this unit representation is generated by the function $\Psi_n\in V^{(n)}\otimes V^{(n)*}$, which corresponds to the unit operator by the canonical isomorphism $V^{(n)}\otimes V^{(n)*}\cong Hom(V^{(n)},V^{(n)})$, and therefore has the form

$$\Psi_n=\sum_{m=0}^{\infty}(\Psi_n^{(e)})_m\otimes(\Psi_n^{(h)})_m. \tag{C6}$$

Substituting Eqs. (C3) and (C4) into Eq. (C6), we obtain a discrete basis set in the space of zero-momentum two-exciton states W_0:

$$\Psi_n=\frac{\sqrt{\pi}}{(2\pi)^2 2^{2n}n!}[(\bar{z}_1-\bar{z}_2)(w_1-w_2)]^n \times\exp\left[-\frac{|z_1|^2+|z_2|^2+|w_1|^2+|w_2|^2}{4} +\frac{(\bar{z}_1+\bar{z}_2)(w_1+w_2)}{4}\right]. \tag{C7}$$

We easily find an alternative a continuous basis set in W_0 which is represented by the functions

$$\Psi_{\mathbf{p}}^{(2)}(\mathbf{r}_1,\mathbf{R}_1,\mathbf{r}_2,\mathbf{R}_2)=\int_0^{2\pi}d\varphi_{\mathbf{p}}\Psi_{\mathbf{p}}(\mathbf{r}_1,\mathbf{R}_1)\Psi_{-\mathbf{p}}(\mathbf{r}_2,\mathbf{R}_2), \tag{C8}$$

where $\Psi_{\mathbf{p}}$ is given by Eq. (4.17), and $\varphi_{\mathbf{p}}$ denotes the angle of $\mathbf{p}$. To find the matrix elements $C_n(\mathbf{p})\equiv\langle\Psi_n|\Psi_{\mathbf{p}}^{(2)}\rangle$ of the transformation between the basis sets, we set $\mathbf{r}_1=\mathbf{r}_2=0$ and $\mathbf{R}_1=-\mathbf{R}_2=\mathbf{R}$, which yields

$$\Psi_{\mathbf{p}}^{(2)}(\mathbf{0},\mathbf{R},\mathbf{0},-\mathbf{R})=\frac{1}{(2\pi)^2}\exp\left[-\frac{p^2}{2}\right]J_0(2pR) =\sum_{n=0}^{\infty}C_n(\mathbf{p})\frac{\sqrt{\pi}}{(2\pi)^2 n!}R^{2n}\exp[-R^2] =\sum_{n=0}^{\infty}|\Psi_n(\mathbf{0},\mathbf{R},\mathbf{0},-\mathbf{R})\rangle\langle\Psi_n|\Psi_{\mathbf{p}}^{(2)}\rangle. \tag{C9}$$

Expanding Eq. (C9) in R, we obtain

$$C_n(\mathbf{p})=\frac{1}{\sqrt{\pi}}\exp\left[-\frac{p^2}{2}\right]L_n(p^2), \tag{C10}$$

where L_n is the Laguerre polynomial:

$$L_n(x)=\sum_{l=0}^{n}(-1)^l x^l\frac{n!}{(l!)^2(n-l)!}. \tag{C11}$$

We can now evaluate the matrix elements

$$H_{mn}=2E_0\delta_{mn}+V_{mn}^{(pp)}+V_{mn}^{(eh)}. \tag{C12}$$

Here we only consider the symmetric Coulomb interaction case $\kappa_{eh}=\kappa_{ee}=0$ for simplicity. We will give the asymmetric part of the Coulomb interaction in Appendix D. $V^{(pp)}$ is proportional to the unit operator on each $V^{(n)}$, $V_{mn}^{(pp)}=\delta_{mn}V_n^{(pp)}$, and

$$2\langle\Psi_m|\frac{\alpha}{|z_1-z_2|}|\Psi_n\rangle=V_m^{(pp)}\delta_{mn} =2\langle(\Psi_n^{(e)})_0|\frac{\alpha}{r_1}|(\Psi_n^{(e)})_0\rangle\delta_{mn}, \tag{C13}$$

where $\Psi_{m0}^{(e)}$ is given by Eq. (C3). The operator $V^{(eh)}$ is diagonal in the $\Psi_{\mathbf{p}}^{(2)}$ basis set, and we therefore have

$$V_{mn}^{(eh)}=2\langle\Psi_m|\frac{-\alpha}{|z_1-w_1|}|\Psi_n\rangle+2\langle\Psi_m|\frac{-\alpha}{|z_1-w_2|}|\Psi_n\rangle \tag{C14}$$

$$=\begin{cases}8\pi\displaystyle\int_0^{\infty}p\,dpU(p)C_n(p)C_m(p) & (m+n=\text{even})\\ 0 & (m+n=\text{odd}),\end{cases} \tag{C15}$$

with $U(p)$ given by the second term of the right-hand side of Eq. (4.18). Calculating the right-hand side of Eqs. (C13) and (C15) yields

$$V_{mn}^{(pp)}=\delta_{mn}2\sqrt{\pi}\frac{(2n-1)!!}{2^{n+1}n!}\alpha, \tag{C16}$$

$$V_{mn}^{(eh)}=-4\alpha\sqrt{\pi/2}\sum_{l_1=0}^{n}\sum_{l_2=0}^{m}(-1)^{l_1+l_2}\frac{(l_1+l_2)!m!n!}{(l_1!l_2!)^2(n-l_1)!(m-l_2)!}\left(\frac{4}{5}\right)^{l_1+l_2+1}F\left(\frac{l_1+l_2+1}{2},\frac{l_1+l_2+2}{2},1,\frac{1}{25}\right), \tag{C17}$$

where F is the hypergeometric function.

Evaluation of two-exciton energy by the two-exciton basis with variational principle is given in Appendix E.

APPENDIX D: EFFECT OF ASYMMETRY OF THE COULOMB INTERACTION

In Appendix C, we obtained the matrix element of the symmetric part of the Coulomb interaction. Here we give the matrix element of the asymmetric part of the Coulomb interaction which is given by Eq. (4.8):

$$\frac{\alpha}{\epsilon(|\mathbf{r}-\mathbf{r}'|)|\mathbf{r}-\mathbf{r}'|}=\frac{\alpha}{|\mathbf{r}-\mathbf{r}'|}e^{-(|\mathbf{r}-\mathbf{r}'|/r_0)^2}. \tag{D1}$$

The asymmetric part of Coulomb interactions $V_{mn}^{A(pp)}$, $U^A(p)$, and $V_{mn}^{A(eh)}$ are given by

$$V_{mn}^{A(pp)}=\delta_{mn}2\sqrt{\pi}\,\frac{(2n-1)!!}{2^{n+1}n!}\alpha\left(\frac{1}{\sqrt{1+(2/r_0)^2}}\right)^{2n+1}. \tag{D2}$$

In this case, $U^A(p)$ is given by

$$U^A(p)=-\alpha\frac{1}{\sqrt{1+2/r_0^2}}\sqrt{\pi/2}\;I_0\left(\frac{p^2}{4(1+2/r_0^2)}\right)\exp\left[-\frac{p^2}{4}\left(\frac{1+4/r_0^2}{1+2/r_0^2}\right)\right]. \tag{D3}$$

Equation (C15) even holds for the asymmetric part of the Coulomb interaction just by replacing $U(p)$ by $U^A(p)$, and we have

$$V_{mn}^{A(eh)}=-4\alpha\sqrt{\pi/2}\frac{1}{\sqrt{1+2/r_0^2}}\sum_{l_1=0}^{n}\sum_{l_2=0}^{m}(-1)^{l_1+l_2}\frac{(l_1+l_2)!m!n!}{(l_1!l_2!)^2(n-l_1)!(m-l_2)!}\left(\frac{4}{5}\right)^{l_1+l_2+1}\left(1+\frac{2}{5r_0^2}\frac{1}{1+2/r_0^2}\right)^{-l_1-l_2-1}$$

$$\times F\left[\frac{l_1+l_2+1}{2},\frac{l_1+l_2+2}{2},1,\frac{1}{25}\frac{1}{(1+2/r_0^2)^2}\left(1+\frac{2}{5r_0^2}\frac{1}{1+2/r_0^2}\right)^{-2}\right]. \tag{D4}$$

The limit $r_0\to\infty$ for Eqs. (D2) and (D4) reproduces Eqs. (C16) and (C17), respectively. The combination of symmetric and asymmetric terms gives the matrix element of the Coulomb interaction (4.8).

APPENDIX E: CALCULATION OF TWO-EXCITON ENERGIES USING THE TWO-EXCITON BASIS SET

We have derived the matrix element of the Coulomb energy of a two-exciton Hamiltonian by a discrete basis set in Sec. IV. Here we will utilize only a continuous basis set in W_0,

$$\Psi_{\mathbf{p}}^{(2)}(\mathbf{r}_1,\mathbf{R}_1,\mathbf{r}_2,\mathbf{R}_2)=\Psi_{\mathbf{p}}(\mathbf{r}_1,\mathbf{R}_1)\Psi_{-\mathbf{p}}(\mathbf{r}_2,\mathbf{R}_2)$$

$$=\frac{1}{(2\pi)^3}\exp\left[-\frac{p^2}{2}\right]\exp\left[-\frac{r_1^2}{4}-\frac{r_2^2}{4}+\frac{i}{2}\mathbf{n}\cdot[\mathbf{r}_1,\mathbf{R}_1]+\frac{i}{2}\mathbf{n}\cdot[\mathbf{r}_2,\mathbf{R}_2]+i\mathbf{p}\cdot(\mathbf{R}_1-\mathbf{R}_2)+\frac{1}{2}\mathbf{n}\cdot[\mathbf{p},(\mathbf{r}_1-\mathbf{r}_2)]\right], \tag{E1}$$

to evaluate the Coulomb energy of the two-exciton for $\kappa_{eh}=\kappa_{ee}=0$. We have to calculate three terms: the electron-electron (hole-hole) Coulomb energy, the electron-hole Coulomb energy in one of the excitons, and the electron-hole Coulomb energy between two different excitons. We denote those as $V^{(pp)}$, $V^{(eh1)}$, and $V^{(eh2)}$ in that order. We have already obtained the expression for $V^{(eh1)}$ in Eq. (4.18),

$$V_{\mathbf{p}'\mathbf{p}}^{(eh1)}=2\frac{1}{\mathcal{N}}\langle\Psi_{\mathbf{p}'}^{(2)}|\frac{\alpha}{|\mathbf{r}_1|}|\Psi_{\mathbf{p}}^{(2)}\rangle$$

$$=-2\frac{1}{\mathcal{N}}\alpha\sqrt{\pi/2}I_0\left(\frac{p^2}{4}\right)\exp\left[-\frac{p^2}{4}\right]$$

$$\times\delta(\mathbf{p}-\mathbf{p}')\frac{1}{(2\pi)^2}\int d\mathbf{R}_2, \tag{E2}$$

where $\mathcal{N}$ is a normalization factor and cancels with $[1/(2\pi)^2]\int d\mathbf{R}_2$. Integration over $\mathbf{R}_2$ appears here explicitly, since we have the same total momentum for initial and final states (the total momentum is 0). The same thing happens for $V^{(pp)}$ and $V^{(eh2)}$. In those cases we find the center-of-mass coordinate $\mathbf{R}_+$ instead of $\mathbf{R}_2$. For calculating $V^{(pp)}$, it is convenient to transform the coordinate from $(\mathbf{R}_1,\mathbf{R}_2,\mathbf{r}_1,\mathbf{r}_2)$ to $(\mathbf{R}_+,\mathbf{r}^e,\mathbf{r}_1,\mathbf{r}_2)$, where $\mathbf{r}^e$ is a vector between two electrons. Then we can carry out all the integration except $\mathbf{R}_+$, and we have

$$V_{\mathbf{p}'\mathbf{p}}^{(pp)}=\langle\Psi_{\mathbf{p}'}^{(2)}|\frac{\alpha}{|\mathbf{r}^e|}|\Psi_{\mathbf{p}}^{(2)}\rangle+\langle\Psi_{\mathbf{p}'}^{(2)}|\frac{\alpha}{|\mathbf{r}^h|}|\Psi_{\mathbf{p}}^{(2)}\rangle$$

$$=\frac{1}{\mathcal{N}}\frac{\alpha}{2\pi}\frac{1}{|\mathbf{p}-\mathbf{p}'|}\exp\left(-\frac{1}{2}|\mathbf{p}-\mathbf{p}'|^2\right)$$

$$\times\{\exp(i\mathbf{n}\cdot[\mathbf{p},\mathbf{p}'])+\exp(-i\mathbf{n}\cdot[\mathbf{p},\mathbf{p}'])\}$$

$$\times\frac{1}{(2\pi)^2}\int d\mathbf{R}_+. \tag{E3}$$

We can perform the similar calculation for $V^{(eh2)}$:

$$V^{(eh2)}_{\mathbf{p}'\mathbf{p}}=2\langle\Psi^{(2)}_{\mathbf{p}'}|\frac{\alpha}{|\mathbf{r}_{12}|}|\Psi^{(2)}_{\mathbf{p}}\rangle$$
$$=-2\frac{1}{\mathcal{N}}\frac{\alpha}{2\pi}\frac{1}{|\mathbf{p}-\mathbf{p}'|}\exp\left(-\frac{1}{2}|\mathbf{p}-\mathbf{p}'|^2\right)$$
$$\times\frac{1}{(2\pi)^2}\int d\mathbf{R}_+, \tag{E4}$$

where $\mathbf{r}_{12}$ is a vector between an electron in one exciton and a hole in the other exciton. So the matrix element of the Coulomb energy for the two-exciton in the continuous basis set is given by

$$V^{(pp)}_{\mathbf{p}'\mathbf{p}}+V^{(eh1)}_{\mathbf{p}'\mathbf{p}}+V^{(eh2)}_{\mathbf{p}'\mathbf{p}}$$
$$=\frac{\alpha}{2\pi}\frac{1}{|\mathbf{p}-\mathbf{p}'|}\exp\left(-\frac{1}{2}|\mathbf{p}-\mathbf{p}'|^2\right)$$
$$\times\{\exp(i\mathbf{n}\cdot[\mathbf{p},\mathbf{p}'])+\exp(-i\mathbf{n}\cdot[\mathbf{p},\mathbf{p}'])\}$$
$$-2\alpha\sqrt{\frac{\pi}{2}}I_0\left(\frac{p^2}{4}\right)\exp\left[-\frac{p^2}{4}\right]\delta(\mathbf{p}-\mathbf{p}')$$
$$-2\frac{\alpha}{2\pi}\frac{1}{|\mathbf{p}-\mathbf{p}'|}\exp\left(-\frac{1}{2}|\mathbf{p}-\mathbf{p}'|^2\right). \tag{E5}$$

Let us evaluate the two-exciton Coulomb energy by a variational principle. As a trial function, we use first a Gaussian type function.

$$\Psi_{p_0}(\mathbf{p})=\sqrt{\frac{2}{\pi}}\frac{1}{p_0}e^{-p^2/p_0^2}. \tag{E6}$$

Then the expectation value becomes

$$\langle\Psi_{p_0}|V^{(pp)}+V^{(eh1)}+V^{(eh2)}|\Psi_{p_0}\rangle$$
$$=2\alpha\sqrt{2\pi}\frac{p_0}{p_0^2+2}-2\alpha\sqrt{2\pi}\frac{1}{\sqrt{4+p_0^2}}-\alpha\sqrt{2\pi}\frac{1}{\sqrt{1+p_0^2}}. \tag{E7}$$

This equation has two minima at $p_0=0$ and ∞. The minimum energy is $-\alpha\sqrt{2\pi}$ which is nothing but twice the one exciton energy.

APPENDIX F: EXCITON SCATTERING MATRIX FOR WEAK AND STRONG COULOMB ASYMMETRY

In this appendix we evaluate the exciton scattering matrix $\overline{\Gamma}^{(2)}(\omega)$ in some limiting cases. We start our analysis with the symmetric case. Straightforward calculation using the continuous representation of Appendix E shows that in this case $U|\phi_0\rangle=0$ (where we have used the notation $\phi_0\equiv\phi(0,0)$). This yields

$$\overline{\Gamma}^{(2)}_{\alpha\beta,\mu\nu}(\omega)=2(\omega-2\epsilon_0+2i\eta)\langle\phi_0|U(\omega-H+2i\eta)^{-1}$$
$$\times(I\overline{I}_{\alpha\beta,\mu\nu}-P\overline{P}_{\alpha\beta,\mu\nu})|\phi_0\rangle=0, \tag{F1}$$

which implies

$$\overline{\Gamma}_{\alpha\beta,\mu\nu}(\omega)=\overline{\Gamma}^{(1)}_{\alpha\beta,\mu\nu}(\omega). \tag{F2}$$

The fact that $\overline{\Gamma}\neq0$ does not contradict the results of Refs. 54 and 53. since on the energy shell ($\omega=2\epsilon_0$) $\overline{\Gamma}^{(1)}$ vanishes. This implies that magnetoexcitons in this case behave like a harmonic system, with nonzero $\chi^{(3)}$ induced by nonlinearities in the dipole operators expanded in powers of boson variables. $\chi^{(3)}$ is then related to a three-level system with equidistant levels but with the ratio of transition dipole between consecutive levels different from $\sqrt{2}$.

We next turn to the weak-asymmetry case $\kappa_{eh}\approx\kappa_{ee}$. To calculate $\overline{\Gamma}^{(2)}$ we use the continuous basis set $|\mathbf{q}\rangle$ [Eq. (E1)]. The operators U and $\overline{F}(\omega)$ are given by the matrix elements $U_{\mathbf{q}\mathbf{q}'}$ represented by Eq. (E5) and

$$[\overline{F}(\omega)]_{\mathbf{q}\mathbf{q}'}=\frac{1}{\omega-2\epsilon_0-2\epsilon_{\mathbf{q}}+2i\eta}\delta_{\mathbf{q}\mathbf{q}'}. \tag{F3}$$

Expanding the middle term in $(\omega-H+2i\eta)^{-1}$ in Eq. (F1) in powers of U, and making use of $[P,H]=0$, we obtain

$$\overline{\Gamma}^{(2)}_{\alpha\beta,\mu\nu}(\omega)=2\omega_0\sum_{n=0}^{\infty}\int\prod_{j=0}^{n}d\mathbf{q}_j\left(\overline{I}_{\alpha\beta,\mu\nu}\frac{1}{\omega_0}U_{0\mathbf{q}_0}-\overline{P}_{\alpha\beta,\mu\nu}\int d\mathbf{q}\frac{1}{2\epsilon_{\mathbf{q}}+\omega_0}U_{\mathbf{q}\mathbf{q}_0}\right)$$
$$\times\prod_{j=1}^{n}\frac{1}{2\epsilon_{\mathbf{q}_j}+\omega_0}U_{\mathbf{q}_{j-1}\mathbf{q}_j}\delta(\mathbf{q}_n) \tag{F4}$$

where $d\mathbf{q}\equiv(2\pi)^{-2}d^2q$, and

$$\omega_0\equiv2\epsilon_0-\omega-2i\eta. \tag{F5}$$

We now note that at large distances r, all Coulomb potentials scale like r^{-1}, whereas in the sum of electron-electron, hole-hole, and electron-hole potentials the r^{-1} terms are canceled. Assuming that the sum of these potentials decays faster than r^{-2}, Eq. (E5) then implies that $U_{\mathbf{p}\mathbf{q}}$ is finite at $\mathbf{p},\mathbf{q}\to0$. On the other hand, due to resonant terms $(\epsilon_{\mathbf{q}}+\omega_0)^{-1}$ in Eq. (F4), the main contribution to the integral at $\omega_0\to0$ comes from the region $\epsilon_{\mathbf{q}_j}\lesssim\omega_0$. This allows us to set $\mathbf{q}_j=0$ in $U_{\mathbf{q}_{j-1}\mathbf{q}_j}$, $U_{0\mathbf{q}_0}$, and $U_{\mathbf{q}\mathbf{q}_0}$ which yields

$$\bar{\Gamma}^{(2)}_{\alpha\beta,\mu\nu}=2g\sum_{n=0}^{\infty}(\bar{I}_{\alpha\beta,\mu\nu}-\bar{P}_{\alpha\beta,\mu\nu}\omega_0 I(\omega_0))[gI(\omega_0)]^n, \tag{F6}$$

where we have used the notation

$$g\equiv\frac{1}{2\pi}U_{00}, \tag{F7}$$

$$I(\omega_0)\equiv\int d\mathbf{q}\frac{1}{2\epsilon_{\mathbf{q}}+\omega_0}. \tag{F8}$$

The integral $I(\omega_0)$ has a logarithmic divergence, the upper cutoff should be at $q\sim 1$ where $U_{\mathbf{qq}'}$ becomes different from U_{00}. We then have

$$I(\omega_0)\simeq-\frac{M}{2\pi}\ln(\omega_0 M), \tag{F9}$$

where M is the effective mass $[2\epsilon_{\mathbf{q}}\approx q^2(2M)^{-1}]$. Substituting Eq. (F9) into Eq. (F6) and performing the summation, we finally obtain

$$\bar{\Gamma}^{(2)}_{\alpha\beta,\mu\nu}(\omega)=2g\frac{\bar{I}_{\alpha\beta,\mu\nu}-M\bar{P}_{\alpha\beta,\mu\nu}(\omega-2\epsilon_0+2i\eta)\ln[(2\epsilon_0-\omega-2i\eta)M]}{1-Mg\ \ln[(2\epsilon_0-\omega-2i\eta)M]}. \tag{F10}$$

Equation (F10) is consistent with the results of Ref. 53 for the exciton scattering amplitude in the weak asymmetry case. Energies of bound biexciton states are given by the poles of $\bar{\Gamma}(\omega)$. Neglecting the damping η in Eq. (F10), for the biexciton energy E_B we obtain

$$1-Mg\ \ln[(2\epsilon_0-E_B)M]=0. \tag{F11}$$

When the distance r_0 on which the r^{-1} terms in the full exciton-exciton potential are canceled is smaller than the exciton size, the energetic parameter given by Eq. (F6) coincides with the parameter G introduced in Ref. 53, and Eq. (F11) coincides with the equation for the biexciton energy derived in Ref. 53. For sufficiently small η and small detuning $|2\epsilon_0-\omega|\ll M^{-1}$, from Eqs. (F11), (5.10), and (5.11) we obtain

$$\bar{\Gamma}_{\alpha\beta,\mu\nu}(\omega)\approx-2M^{-1}\{\ln[(2\epsilon_0-\omega)M]\}^{-1}\bar{I}_{\alpha\beta,\mu\nu}. \tag{F12}$$

Equation (F12) gives the off-shell exciton scattering matrix at $\mathbf{k}=0$. Since this matrix has a weak dependence on $\mathbf{k}$, the on-shell scattering matrix $\bar{\Gamma}(\mathbf{k})$ is given by $\bar{\Gamma}(\omega)$ if we set $\omega=2\epsilon_0+k^2/M$ which yields $\bar{\Gamma}(k)\sim(\ln k)^{-1}$. Upon switching from plane to spherical waves for the initial wave, this gives the scattering amplitude $S(\mathbf{k})\sim(\sqrt{k}\ln k)^{-1}$, in agreement with Ref. 53

Finally, consider the case of strong asymmetry related to weak electron-hole interaction. Neglecting the electron-hole interaction in zero order we obtain

$$\bar{\Gamma}^{(2)}_{\alpha\beta,\mu\nu}=2(\omega-2\epsilon_0+2i\eta)\sum_n\frac{E_n}{\omega-E_n+2i\eta}\times[\bar{I}_{\alpha\beta,\mu\nu}-(-1)^n\bar{P}_{\alpha\beta,\mu\nu}], \tag{F13}$$

where $E_n\equiv V^{(pp)}_{nn}$ is given by Eq. (4.8), with Eqs. (C16) and (D2), and for large n, $E_n\sim n^{-1/2}$. This means that $\mathrm{Im}\bar{\Gamma}^{(2)}$ has a logarithmic divergence. However as indicated earlier, at large distances all potentials are the same. We denote the characteristic length on which the electron-hole potential becomes comparable to the particle-particle potential by r_0. Since n is of the system's area, the sum in Eq. (F13) should be truncated at $n\sim r_0^2$, and we have

$$\bar{\Gamma}^{(2)}_{\alpha\beta,\mu\nu}(\omega)=2(\omega-2\epsilon_0+2i\eta)\sum_{n=0}^{r_0^2}\frac{E_n}{\omega-E_n+2i\eta}\times[\bar{I}_{\alpha\beta,\mu\nu}-(-1)^n\bar{P}_{\alpha\beta,\mu\nu}]. \tag{F14}$$

APPENDIX G: EXPRESSION FOR $\bar{P}_{\alpha\beta,\mu\nu}$

In this appendix the matrix elements of the electron-spin permutation $\bar{P}_{\alpha\beta,\mu\nu}$ given in Sec. V are evaluated. We employed the model where electron and hole have total angular momenta $\frac{1}{2}$ and $\frac{3}{2}$, respectively. The total angular momentum part of the wave function of the electron and hole are written as $e_{(1/2)m}$ $(m=\pm\frac{1}{2})$ and $h_{(3/2)n}$ $(n=\pm 3/2)$. Then the angular momentum part of the exciton wave function $\phi_{1,\pm 1}$ is given by the combination of the angular momentum of electron and hole:

$$\phi_{1,\pm 1}(1)=e_{1/2,\mp 1/2}(1)h_{3/2,\pm 3/2}(1). \tag{G1}$$

The angular momentum part of two-exciton states χ are given by the combination of these $\phi_{1,\pm1}$,

$$\chi_{2,\pm2}=\phi_{1,\pm1}(1)\phi_{1,\pm1}(2),$$

$$\chi_{2,0}=\frac{1}{\sqrt{2}}\{\phi_{1,1}(1)\phi_{1,-1}(2)+\phi_{1,-1}(1)\phi_{1,1}(2)\}, \quad \text{(G2)}$$

$$\chi_{1,0}=\frac{1}{\sqrt{2}}\{\phi_{1,1}(1)\phi_{1,-1}(2)-\phi_{1,-1}(1)\phi_{1,1}(2)\},$$

where the argument in the parentheses indicates the numbering of each electron (or hole). The permutation operator $\overline{P}$ is composed of two parts, $\overline{P}=(\overline{P_e}+\overline{P_h})/2$, where $\overline{P_e}$ represents the exchange of electrons and $\overline{P_h}$ represents the exchange of holes.

$$\overline{P_e}\chi_{2,\pm2}=\overline{P_h}\chi_{2,\pm2}=\chi_{2,\pm2}, \quad \text{(G3)}$$

$$\overline{P_e}\chi_{2,0}=\frac{1}{\sqrt{2}}[e_{1/2,1/2}(1)h_{3/2,3/2}(1)e_{1/2,-1/2}(2)h_{3/2,-3/2}(2)+e_{1/2,-1/2}(1)h_{3/2,-3/2}(1)e_{1/2,1/2}(2)h_{3/2,3/2}(2)], \quad \text{(G4)}$$

$$\overline{P_h}\chi_{2,0}=\frac{1}{\sqrt{2}}[e_{1/2,-1/2}(1)h_{3/2,-3/2}(1)e_{1/2,1/2}(2)h_{3/2,3/2}(2)+e_{1/2,1/2}(1)h_{3/2,3/2}(1)e_{1/2,-1/2}(2)h_{3/2,-3/2}(2)]. \quad \text{(G5)}$$

We can obtain $\overline{P_e}\chi_{1,0}$ and $\overline{P_h}\chi_{1,0}$ by changing the sign of the second term of the right-hand side of Eqs. (G4) and (G5), respectively. These wave functions are mapped on the basis formed by $\chi_{2,2}$, $\chi_{2,-2}$, $\chi_{2,0}$, and $\chi_{1,0}$ and we have

$$\overline{P}=\begin{pmatrix}1&0&0&0\\0&1&0&0\\0&0&0&0\\0&0&0&0\end{pmatrix}. \quad \text{(G6)}$$

The matrix $\overline{P}_{\alpha\beta,\mu\nu}$ is written by a basis set: $\phi_{1,1}(1)\phi_{1,1}(2)$, $\phi_{1,-1}(1)\phi_{1,-1}(2)$, $\phi_{1,1}(1)\phi_{1,-1}(2)$, and $\phi_{1,-1}(1)\phi_{1,1}(2)$. After the transformation in this basis set we have a expression for $P_{\alpha\beta,\mu\nu}$, and it has the same form as Eq. (G6).

[1] G. Bastard, *Wave Mechanics Applied to Semiconductor Heterostructures* (Les Editions de Physique, Paris, 1988).

[2] H. Haug and S. W. Koch, *Quantum Theory of the Optical and Electronic Properties of Semiconductors*, 3rd ed. (World Scientific, Singapore, 1994).

[3] L. Banyai and S. W. Koch, *Semiconductor Quantum Dots* (World Scientific, Singapore, 1993).

[4] *Optics of Semiconductor Nanostructures*, edited by F. Henneberger, S. Schmitt-Rink, and E. O. Göbel (Akademie Verlag, Berlin, 1993).

[5] A. P. Alivisatos, Science **271**, 933 (1996).

[6] J. Bleuse, G. Bastard, and P. Voison, Phys. Rev. Lett. **60**, 220 (1988).

[7] M. M. Dignam and J. E. Sipe, Phys. Rev. Lett. **64**, 1797 (1990); Phys. Rev. B **43**, 4097 (1991).

[8] T. Meier, F. Rossi, P. Thomas, and S. W. Koch, Phys. Rev. Lett. **75**, 2558 (1995).

[9] U. Siegner, M.-A. Mycek, S. Glutsch, and D. S. Chemla, Phys. Rev. Lett. **74**, 470 (1995).

[10] U. Siegner, M.-A. Mycek, S. Glutsch, and D. S. Chemla, Phys. Rev. Lett. **51**, 4953 (1995).

[11] P. Kner, S. Bar-Ad, M. V. Marquezini, D. S. Chemla, and W. Schäfer, Phys. Rev. Lett. **78**, 1319 (1997).

[12] J. B. Stark, W. H. Knox, D. S. Chemla, W. Schäfer, S. Schmitt-Rink, and C. Stafford, Phys. Rev. Lett. **65**, 3033 (1990).

[13] T. Rappen, J. Schröder, A. Leisse, M. Wegener, W. Schäfer, N. J. Sauer, and T. Y. Chang, Phys. Rev. B **44**, 13 093 (1991).

[14] S. T. Cundiff, M. Koch, W. H. Knox, J. Shah, and W. Stolz, Phys. Rev. Lett. **77**, 1107 (1996).

[15] M. Jiang, H. Wang, R. Merlin, D. G. Steel, and D. Cardona, Phys. Rev. B **48**, 15 476 (1993).

[16] S.-R. Eric Yang and L. J. Sham, Phys. Rev. Lett. **58**, 2598 (1987).

[17] C. Stafford, S. Schmitt-Rink, and W. Schäfer, Phys. Rev. B **41**, 10 000 (1990).

[18] S. Glutsch and D. S. Chemla, Phys. Rev. B **52**, 8317 (1995).

[19] T. Meier, A. Schulze, P. Thomas, H. Vaupel, and K. Maschke, Phys. Rev. B **51**, 13 977 (1995).

[20] W. Huhn and A. Stahl, Phys. Status Solidi B **124**, 167 (1984).

[21] S. Schmitt-Rink, D. S. Chemla, and H. Haug, Phys. Rev. B **37**, 941 (1988).

[22] M. Lindberg and S. W. Koch, Phys. Rev. B **38**, 3342 (1988).

[23] H. Wang, K. B. Ferrio, D. G. Steel, Y. Z. Hu, R. Binder, and S. W. Koch, Phys. Rev. Lett. **71**, 1261 (1993).

[24] H. Wang, K. B. Ferrio, D. G. Steel, P. R. Berman, Y. Z. Hu, R. Binder, and S. W. Koch, Phys. Rev. A **49**, 1551 (1994).

[25] Y. Z. Hu, R. Binder, S. W. Koch, S. T. Cundiff, H. Wang, and D. G. Steel, Phys. Rev. B **49**, 14 382 (1994).

[26] T. Rappen, U. G. Peter, M. Wegener, and W. Schäfer, Phys. Rev. B **49**, 10 774 (1994).

[27] M. Lindberg, Y. Z. Hu, R. Binder, and S. W. Koch, Phys. Rev. B **50**, 18 060 (1994).
[28] V. M. Axt, A. Stahl, E. J. Mayer, P. Haring Bolivar, S. Nüsse, K. Ploog, and K. Köhler, Phys. Status Solidi B **188**, 447 (1995).
[29] W. Schäfer, D. S. Kim, J. Shah, T. C. Damen, J. E. Cunningham, K. W. Goossen, L. N. Pfeiffer, and K. Köhler, Phys. Rev. B **53**, 16 429 (1996).
[30] K. Bott, O. Heller, D. Bennhardt, S. T. Cundiff, P. Thomas, E. J. Mayer, G. O. Smith, R. Eccleston, J. Kuhl, and K. Ploog, Phys. Rev. B **48**, 17 418 (1993).
[31] B. F. Feuerbacher, J. Kuhl, and K. Ploog, Phys. Rev. B **43**, 2439 (1991).
[32] S. Bar-Ad and I. Bar-Joseph, Phys. Rev. Lett. **68**, 349 (1992).
[33] D. J. Lovering, R. T. Phillips, G. J. Denton, and G. W. Smith, Phys. Rev. Lett. **68**, 1880 (1992).
[34] K.-H. Pantke, D. Oberhauser, V. G. Lyssenko, J. M. Hvam, and G. Weimann, Phys. Rev. B **47**, 2413 (1993).
[35] E. J. Mayer, G. O. Smith, V. Heuckeroth, J. Kuhl, K. Bott, A. Schulze, T. Meier, D. Bennhardt, S. W. Koch, P. Thomas, R. Hey, and K. Ploog, Phys. Rev. B **50**, 14 730 (1994).
[36] E. J. Mayer, G. O. Smith, V. Heuckeroth, J. Kuhl, K. Bott, A. Schulze, T. Meier, S. W. Koch, P. Thomas, R. Hey, and K. Ploog, Phys. Rev. B **51**, 10 909 (1995).
[37] S. Mukamel, *Principles of Nonlinear Optical Spectroscopy* (Oxford, University Press, New York, 1995).
[38] F. C. Spano and S. Mukamel, Phys. Rev. Lett. **66**, 1197 (1991); J. Chem. Phys. **95**, 7526 (1991).
[39] J. A. Leegwater and S. Mukamel, Phys. Rev. A **46**, 452 (1992).
[40] V. Chernyak and S. Mukamel, Phys. Rev. B **48**, 2470 (1993).
[41] V. Chernyak and S. Mukamel, J. Chem. Phys. **100**, 2953 (1994).
[42] J. Knoester and S. Mukamel, Phys. Rep. **205**, 1 (1991).
[43] O. Dubovsky and S. Mukamel, J. Chem. Phys. **95**, 7828 (1991).
[44] V. Chernyak, N. Wang, and S. Mukamel, Phys. Rep. **263**, 213 (1995).
[45] T. Meier, V. Chernyak, and S. Mukamel, J. Phys. Chem. B **101**, 7332 (1997); W. M. Zhang, T. Meier, V. Chernyak, and S. Mukamel, J. Chem. Phys. **108**, 7763 (1998).
[46] *Lectures in Theoretical Physics*, edited by W. E. Brittin, B. W. Downs, and J. Downs (Interscience, New York, 1961), Vol. 3, p. 106; R. Zwanzig, Physica (Amsterdam) **30**, 1109 (1964); H. Mori, Prog. Theor. Phys. **33**, 423 (1965); Prog. Theor. Phys. **34**, 399 (1965).
[47] V. M. Axt and A. Stahl, Z. Phys. B **93**, 195 (1994).
[48] V. M. Axt and A. Stahl, Z. Phys. B **93**, 205 (1994).
[49] K. Victor, V. M. Axt, and A. Stahl, Phys. Rev. B **51**, 14 164 (1995).
[50] M. Z. Maialle and L. J. Sham, Phys. Rev. Lett. **73**, 3310 (1994).
[51] Th. Östreich, K. Schönhammer, and L. J. Sham, Phys. Rev. Lett. **74**, 4698 (1995).
[52] V. Chernyak and S. Mukamel, J. Opt. Soc. Am. B **13**, 1302 (1996).
[53] Yu. A. Bychkov and E. I. Rashba, Zh. Eksp. Teor. Fiz. **85**, 1826 (1983) [Sov. Phys. JETP **58**, 1062 (1983)].
[54] I. V. Lerner and Yu. E. Lozovik, Zh. Eksp. Teor. Fiz. **82**, 1188 (1982) [Sov. Phys. JETP **55**, 691 (1982)].
[55] O. Kuhn, V. Chernyak, and S. Mukamel, J. Chem. Phys. **105**, 8586 (1996).
[56] D. S. Chemla, J.-Y. Bigot, M.-A. Mycek, S. Weiss, and W. Schäfer, Phys. Rev. B **50**, 8439 (1994).
[57] M. Lindberg, R. Binder, and S. W. Koch, Phys. Rev. A **45**, 1865 (1992).
[58] R. Zimmermann, Phys. Status Solidi B **173**, 129 (1992).
[59] A. A. Kirillov, *Elements of the Theory of Representations* (Springer-Verlag, Berlin, 1976).
[60] M. E. Portnoi and E. I. Rashba, Phys. Rev. B **54**, 13 791 (1996).